Chem Soc Rev

Chemical Society Reviews

www.rsc.org/chemsocrev

Volume 37 | Number 11 | November 2008 | Pages 2361–2580

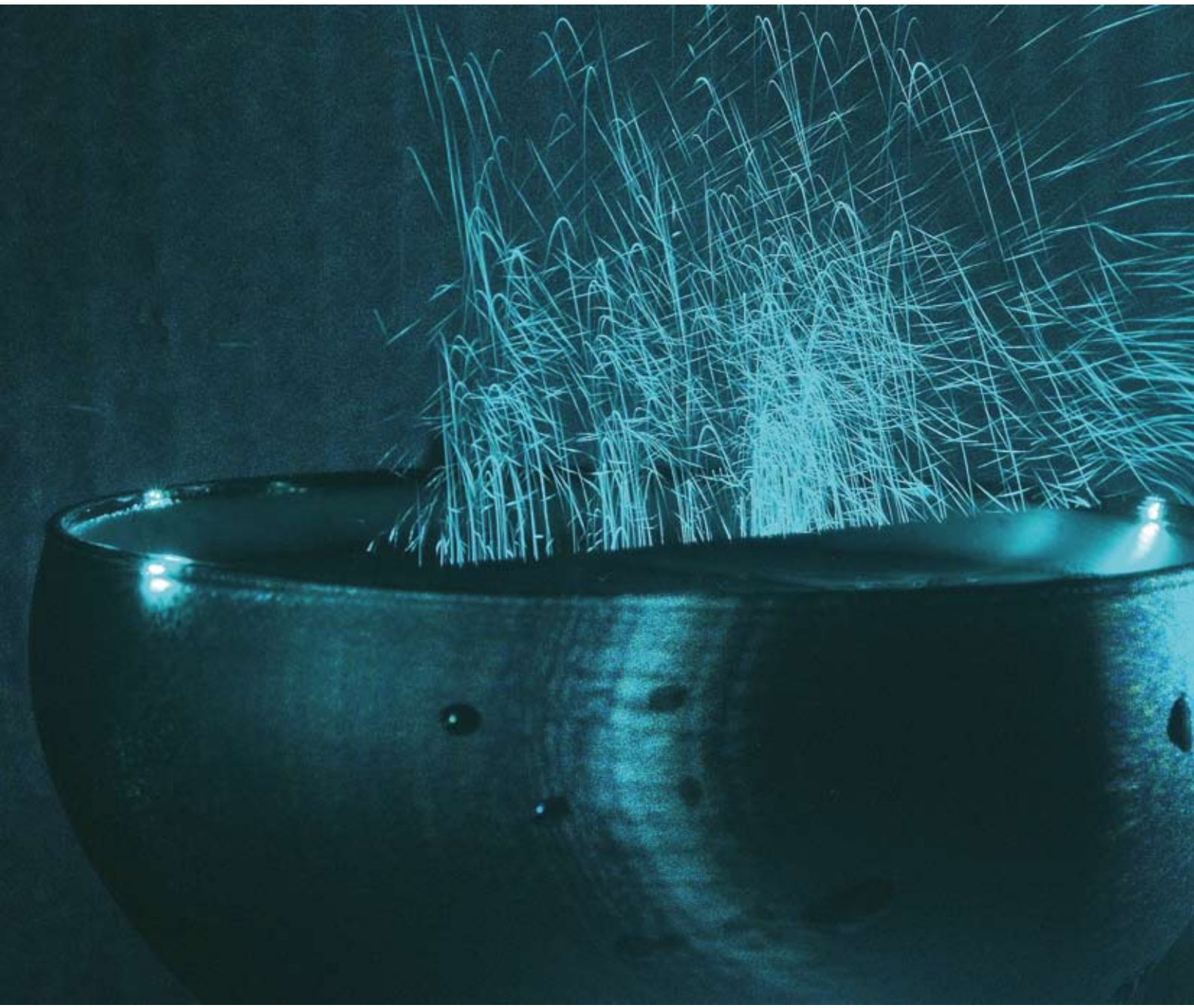

ISSN 0306-0012

CRITICAL REVIEW
Gérard Liger-Belair, Guillaume Polidori and Philippe Jeandet
Recent advances in the science of champagne bubbles

TUTORIAL REVIEW
Ariel Fernández and Alejandro Crespo
Protein wrapping: a molecular marker for association, aggregation and drug design

RSC Publishing

0306-0012(2008)37:11;1-T

Recent advances in the science of champagne bubbles

Gérard Liger-Belair,*[a] Guillaume Polidori[b] and Philippe Jeandet[a]

Received 8th July 2008
First published as an Advance Article on the web 5th September 2008
DOI: 10.1039/b717798b

The so-called *effervescence* process, which enlivens champagne and sparkling wines tasting, is the result of the fine interplay between CO_2-dissolved gas molecules, tiny air pockets trapped within microscopic particles during the pouring process, and some liquid properties. This *critical review* summarizes recent advances obtained during the past decade concerning the physicochemical processes behind the nucleation, rise, and burst of bubbles found in glasses poured with champagne and sparkling wines. Those phenomena observed in close-up through high-speed photography are often visually appealing. Let's hope that your enjoyment of champagne will be enhanced after reading this fully illustrated review dedicated to the deep beauties of nature often hidden behind many everyday phenomena (51 references).

1. Introduction

From a strictly chemical point of view, champagne and sparkling wines are multicomponent hydroalcoholic systems supersaturated with CO_2-dissolved gas molecules (formed together with ethanol during the fermentation process).[1] As soon as a bottle of champagne or sparkling wine is uncorked, the progressive release of CO_2-dissolved gas molecules is responsible for bubble formation, the so-called effervescence process. It is worth noting that approximately five litres of CO_2 must escape from a typical 0.75 L champagne bottle. To get an idea of how many bubbles are potentially involved throughout the degassing process from this single bottle, we can divide this volume of CO_2 to be released by the average volume of a typical bubble of 0.5 mm in diameter. A huge number close to 10^8 is found! Actually, champagne and sparkling wine tasting mainly differs from still non-effervescent wine tasting due to the presence of those myriad of bubbles continuously rising through the liquid medium. This is the reason why considerable efforts have been conducted the past few years in order to better illustrate, detect, understand and finally control each and every parameter involved in the bubbling process. Without bubbles, champagne and other sparkling wines would be unrecognizable as such (see Fig. 1), but the role of effervescence goes far beyond the solely aesthetical point of view... This critical review covers recent progress in the field of champagne science.

[a] *Laboratoire d'Œnologie et Chimie Appliquée, Unité de Recherche sur la Vigne et le Vin de Champagne (URVVC), Université de Reims Champagne-Ardenne, B.P. 1039, 51687 Reims Cedex 2, France. E-mail: gerard.liger-belair@univ-reims.fr; Fax: 00 (33)3 26 91 86 14; Tel: 00 (33)3 26 91 86 14*
[b] *Laboratoire de Thermomécanique, Groupe de Recherche en Sciences Pour l'Ingénieur (GRESPI), Université de Reims Champagne-Ardenne, B.P. 1039, 51687 Reims Cedex 2, France*

Gérard Liger-Belair

Gérard Liger-Belair was born in Beyrouth (Lebanon) in 1970. He studied Fundamental Physics in Paris VI University. He received his PhD in Physical Sciences in 2001, from Reims University, where he was appointed Associate Professor in 2002 and full Professor of Chemical Physics in 2007. He is presently the leader of the "Bubble Team" in the Laboratory of Enology and Applied Chemistry. He has been researching the physics and chemistry behind the bubbling properties of carbonated beverages (including champagne, sparkling wines, beers and fizzy waters) for several years. He is the author or co-author of many articles and books upon the subject. He is the recipients of several scientific awards and recognitions, including the 2004 Award for Professional/Scholarly book in Physics from the Association of American Publishers for his book "Uncorked, the science of champagne", published in 2004 by Princeton University Press. He also has a passion for micro-photography. His series of "bubble" photographs, at the juncture between pure Science and modern Art, have appeared in numerous exhibitions and art galleries. His current interests include the science of bubbles, foams and thin films, and their broad interdisciplinary applications.

2. Within a champagne bottle

2.1. Where do CO_2 molecules dissolved in champagne come from?

The modern production of champagne is not so far removed from that empirically developed by the Benedictine monk dom Pierre Pérignon in the late 17th century. This method is also used outside the Champagne region. Sparkling wines produced as such are labelled *méthode traditionnelle*. Indeed, most American and Australian sparkling winemakers use this method to elaborate their own sparkling wines. This method involves several distinct steps:

A first alcoholic fermentation. Three types of noble grapes are grown in the 75 000 acres of the Champagne vineyards:

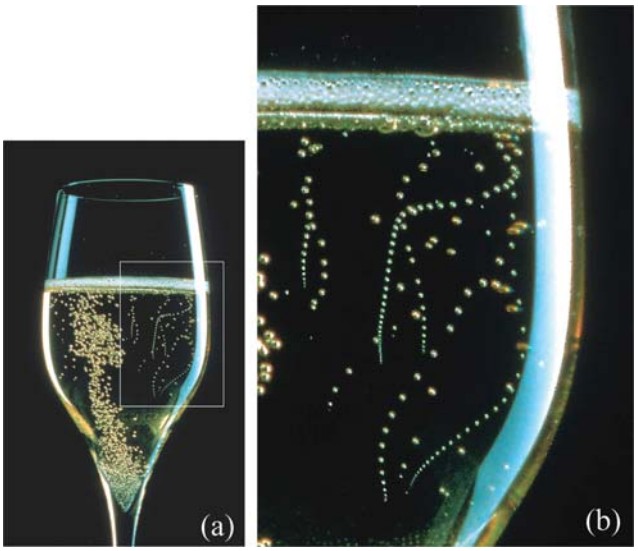

Fig. 1 Photograph of a typical flute poured with champagne (a), and close-up on particles acting as bubble nucleation sites freely floating in the bulk of the flute (called *fliers*), thus creating charming bubble trains in motion in the champagne bulk (b) (© Alain Cornu/Collection CIVC).

Chardonnay (a white grape), *Pinot Meunier*, and *Pinot Noir* (both dark grapes). Usually around mid-September, the grapes harvested from these vineyards are pressed to make a juice, called "the grape must". After pressing, the must is transferred into an open vat where yeast (a kind of fungus called *Saccharomyces cerevisiae*) is added. Generally speaking, the key chemical reaction of winemaking is alcoholic fermentation: the conversion of sugars into ethanol and carbon dioxide by yeast. The process of fermentation was first scientifically described by the French chemist Joseph-Louis Gay Lussac, in 1810, when he demonstrated that glucose is the basic starting block for producing ethanol:

$$C_6H_{12}O_6 \rightarrow 2CH_3CH_2OH + 2CO_2 \qquad (1)$$

The manner in which yeast contributes to the fermentation process was not clearly understood until 1857, when the French microbiologist Louis Pasteur discovered that not only does the fermentation process not *require* any oxygen, but alcohol yield is actually *reduced* by its presence. The amount of ethanol generated by this first alcoholic fermentation is about 11%. At this step, "champagne" is still actually a non-effervescent white wine, because the carbon dioxide produced during the first alcoholic fermentation is allowed to escape into the atmosphere.

The art of blending. Because it is rare that a single wine of a single vintage from a single vineyard and grape variety will provide the perfect balance of flavour, sugar level, and acidity necessary for making a fine champagne, winemakers will often mix several different still wines. This is called the *assemblage* (or blending) step, and it is carried out directly after the first alcoholic fermentation is complete. Blending is considered the key to the art of champagne-making. A cellar master will sometimes blend up to 80 different wines from various grape varieties, vineyards and vintages to produce one champagne. The blending of still wines originally made from the three kinds of grapes forms a base wine, which will then undergo a second fermentation—the key step in producing the "sparkle" in champagne and sparkling wines.

The *prise de mousse*: a second alcoholic fermentation. Once the base wine is created, sugar (about 24 grams per litre) and yeast are added. The entire concoction is put into thick-walled glass bottles and sealed with caps. The bottles are then placed in a cool cellar (12 to 14 °C), and the wine is allowed to slowly ferment for a second time, producing alcohol and carbon dioxide again. Actually, during this second fermentation process which occurs in cool cellars, the bottles are sealed, so that the CO_2 molecules cannot escape and they progressively dissolve into the wine. Therefore, CO_2-dissolved molecules in the wine and gaseous CO_2 molecules under the cork progressively establish an equilibrium—an application of Henry's law which states that the partial pressure of a given gas above a solution is proportional to the concentration of the gas dissolved in the solution, as expressed by the following relationship:

$$c = k_H P_{CO_2} \qquad (2)$$

where c is the concentration of dissolved CO_2 molecules, P_{CO_2} is the partial pressure of CO_2 molecules in the vapor phase, and k_H is the Henry's law constant. For a given gas, k_H is strongly temperature-dependent. The lower the temperature, the higher the Henry's law constant, and therefore the higher the solubility.

In champagne and sparkling wines, Agabaliantz thoroughly examined the solubility of dissolved CO_2 molecules as a function of both temperature and wine parameters.[2] His empirical relationships are still used nowadays by champagne and sparkling winemakers. For a typical sparkling wine elaborated according to the *méthode traditionnelle*, Agabaliantz established the temperature dependence of the Henry's law constant, which is displayed in Table 1. Thermodynamically speaking, the behaviour of Henry's law constant as a function of temperature can be conveniently expressed with a Van't Hoff like equation as follows:

$$k_H(\theta) = k_{298\,K} \exp\left[-\frac{\Delta H_{diss}}{\Re}\left(\frac{1}{\theta} - \frac{1}{298}\right)\right] \qquad (3)$$

where ΔH_{diss} is the dissolution enthalpy of CO_2 molecules in the liquid medium (in J mol^{-1}), $\Re$ is the ideal gas constant (8.31 J K^{-1} mol^{-1}), and θ is the absolute temperature (in K). By fitting Agabaliantz data with the latter equation, it is worth noting that the dissolution enthalpy of CO_2 molecules in champagne may be evaluated.[3] The best fit to Agabaliantz data was found with $\Delta H_{diss} \approx 24\,800$ J mol^{-1} (see Fig. 2). In comparison, the dissolution enthalpy of CO_2 molecules in pure water is about 19 900 J mol^{-1}.[4]

2.2. The pressure under the cork

Following eqn (1), 24 grams per litre of sugar added in closed bottles to promote the second alcoholic fermentation produce approximately 11.8 grams per litre of CO_2 within each bottle. Therefore, a typical 75 cL champagne bottle contains close to 9 g of CO_2 molecules. By use of the molar mass of CO_2

Table 1 Henry's law constant for CO_2 in champagne as a function of temperature, for a typical champagne with 12.5% (v/v) of ethanol and 10 g L^{-1} of sugars (compiled from the data by Agabaliantz[2])

Temperature/°C	Henry's law constant k_H/kg m^{-3} atm^{-1}
0	2.98
1	2.88
2	2.78
3	2.68
4	2.59
5	2.49
6	2.41
7	2.32
8	2.23
9	2.16
10	2.07
11	2.00
12	1.93
13	1.86
14	1.79
15	1.73
16	1.67
17	1.60
18	1.54
19	1.48
20	1.44
21	1.40
22	1.34
23	1.29
24	1.25
25	1.21

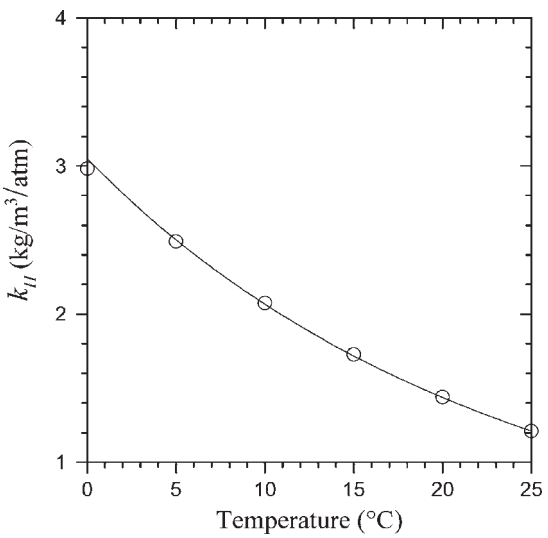

Fig. 2 Henry's law constant as a function of temperature (○) (redrawn from Agabaliantz data[2]); the line is the best fit to Agabaliantz data, drawn with the Van't Hoff like eqn (3) and with $\Delta H_{diss} \approx 24\,800$ J mol^{-1}.

(44 g mol^{-1}), and the molar volume of an ideal gas (close to 24 L mol^{-1} at 12 °C), it can be deduced that about 5 L of gaseous CO_2 are trapped into a single bottle of champagne (*i.e.*, 6 times its own volume!).

Because the solubility of CO_2 strongly depends on the champagne temperature, the pressure of gaseous CO_2 under the cork also strongly depends, in turn, on the champagne temperature. The physicochemical equilibrium of CO_2 molecules within a champagne bottle is ruled by both Henry's law (for CO_2-dissolved gas molecules) and the ideal gas law (for the gaseous CO_2 in the headspace under the cork). Moreover, the conservation of the total mass of CO_2 molecules (dissolved into the wine and in the vapor phase under the cork) applies, since bottles are hermetically closed. Therefore, by combining the two above-mentioned laws with mass conservation, the following relationship can easily be determined which links the pressure P of gaseous CO_2 under the cork (in bars) with both temperature and the bottle's parameters as:

$$P \approx \frac{m\Re\theta}{4.4 \times 10^3 v + (k_H \Re\theta) V} \quad (4)$$

where m is the total mass of CO_2 within the bottle (in grams), θ is the champagne temperature (in K), $\Re$ is the ideal gas constant (8.31 J K^{-1} mol^{-1}), k_H is the Henry's law constant given in Table 1 (in grams per litre per bar), V is volume of champagne within the bottle (in litres), and v is the volume of the gaseous headspace under the cork (in litres).

For a typical champagne bottle with $V = 75$ cL, a volume in the headspace of $v = 25$ mL, and a total mass of CO_2 trapped within the bottle of $m = 9$ g, the variation in the pressure P under the cork with the champagne temperature θ is displayed in Fig. 3. At the temperature of champagne tasting (usually between 8 and 10 °C), the pressure within a typical 75 cL champagne bottle is close to 5 bars (*i.e.*, 5×10^5 N m^{-2}).

2.3. The chemical composition of champagne

From the point of view of the chemist, champagne can indeed be viewed as a multicomponent aqueous solution. The fine chemical composition of a typical Champagne wine is reported in Table 2.[5] Actually, gases like CO_2 undergo specific reactions with water. Equilibrium is established between the dissolved $(CO_2)_{aq}$ and H_2CO_3, the carbonic acid:

$$(CO_2)_{aq} + H_2O \leftrightarrow H_2CO_3 \quad (5)$$

Moreover, carbonic acid is a weak acid that dissociates in two steps:

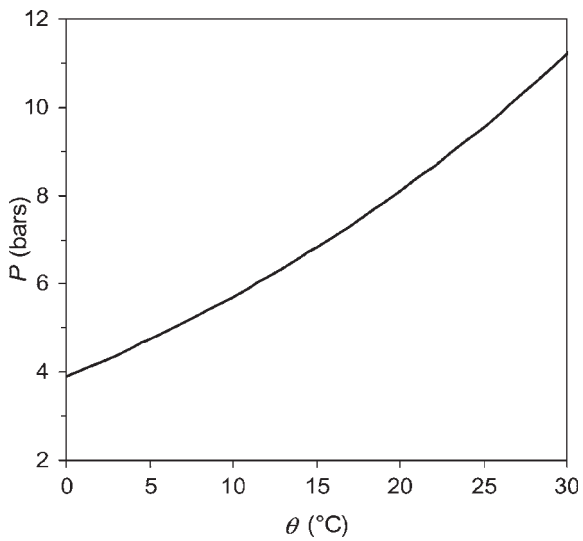

Fig. 3 Pressure of gaseous CO_2 under the cork of a typical 75 cL champagne bottle as a function of champagne temperature.

Table 2 Average composition of a typical Champagne wine.[5] Typically, pH ≈ 3.2 and the ionic strength is 0.02 M

Compound	Quantity
Ethanol	≈12.5% v/v
CO_2	10–12 g L^{-1}
Glycerol	≈5 g L^{-1}
Tartaric acid	≈2.5 to 4 g L^{-1}
Lactic acid	≈4 g L^{-1}
Sugars	10–50 g L^{-1}
Proteins	5–10 mg L^{-1}
Polysaccharides	≈200 mg L^{-1}
Polyphenols	≈100 mg L^{-1}
Amino acids	0.8–2 mg L^{-1}
Volatile organic compounds (VOC)	≈700 mg L^{-1}
Lipids	≈10 mg L^{-1}
K^+	200–450 mg L^{-1}
Ca^{2+}	60–120 mg L^{-1}
Mg^{2+}	50–90 mg L^{-1}
SO_4^{2-}	≈200 mg L^{-1}
Cl^-	≈10 mg L^{-1}

$$H_2CO_3 + H_2O \leftrightarrow H_3O^+ + HCO_3^- \quad p\mathit{K}_{a1}\ (\text{at } 25\ ^\circ\text{C}) = 6.37 \tag{6}$$

$$HCO_3^- + H_2O \leftrightarrow H_3O^+ + CO_3^{2-} \quad p\mathit{K}_{a2}\ (\text{at } 25\ ^\circ\text{C}) = 10.25 \tag{7}$$

However, as the pH of champagne and sparkling wines is relatively low (in the order of 3.2), no carbonated species (CO_3^{2-}, HCO_3^-) should coexist with dissolved CO_2. Recently, the ^{13}C nuclear magnetic resonance (NMR) spectroscopy technique was used as an unintrusive and non-destructive method to determine the amount of CO_2 dissolved in closed bottles of champagne and sparkling wines.[6] Different well-separated peaks were recorded in a ^{13}C spectrum, as can be seen in Fig. 4: (i) the quadruplet of CH_3 group of ethanol appears at 17.9 ppm, (ii) the triplet of the CH_2(–OH) group of ethanol at 57.3 ppm, and (iii) the singlet of CO_2 appears at 124.4 ppm, thus confirming the absence of other carbonated species (CO_3^{2-}, HCO_3^-) in the liquid matrix (contrary to fizzy waters for example, where pH values near neutrality enable the above mentioned carbonated species to cohabit with CO_2-dissolved gas molecules).

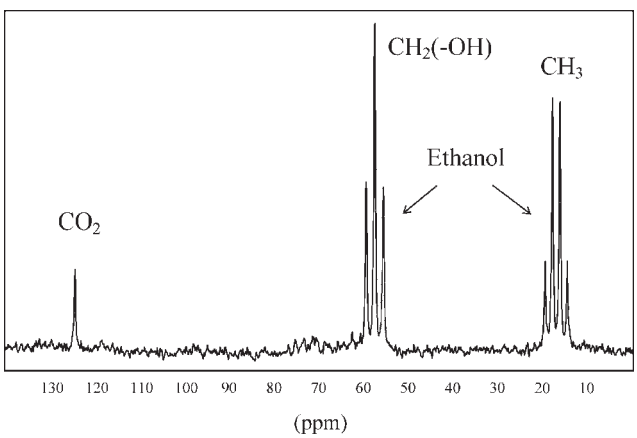

Fig. 4 ^{13}C spectrum recorded to measure the CO_2 concentration in a typical Champagne wine;[6] it is clear that no carbonated species (CO_3^{2-}, HCO_3^-) coexist with dissolved CO_2.

2.4. Uncorking the bottle

Have you ever thought about the velocity reached by an uncontrolled champagne cork popping out of a bottle? Measurements conducted in our laboratory in Reims led to typical velocities ranging from 50 to 60 km h^{-1}.[1] So, if it hits someone in the eye, it could do some serious harm and dramatically change the course of any romantic evening you might have planned... When opening a bottle of champagne (or carbonated beverage in general), everyone would have already noticed the cloud of fog forming right above the bottle neck (as wonderfully illustrated by the photograph displayed in Fig. 5 taken by Jacques Honvault, a master of high-speed photography). This cloud of fog is due to a significant drop in temperature in the headspace below the champagne surface, caused by the sudden gas expansion when the bottle is uncorked. Actually, this sudden temperature drop is responsible for the instantaneous condensation of water vapor into the form of this characteristic cloud of fog. Assuming an adiabatic expansion experienced by the gas volume of the headspace (from about 5 atm to 1 atm), the corresponding theoretical drop in temperature experienced by the gas volume may easily be accessed by the following and well-known relationship:

$$P^{(1-\Gamma)}\theta^{\Gamma} = \text{constant} \tag{8}$$

where P, θ, and Γ are the pressure, temperature, and ratio of specific heats of the gas volume experiencing adiabatic expansion, respectively. With the ratio of specific heats for CO_2

Fig. 5 Uncontrolled champagne cork popping out of a bottle; the cloud of fog forming right above the bottle neck clearly appears. (Photograph by Jacques Honvault.)

molecules being 1.3, an adiabatic expansion from about 5 atm to 1 atm when uncorking the bottle corresponds to a theoretical drop in temperature close to 90 °C! No wonder traces of water vapor immediately condensate into the form of a small cloud.

In addition to this sudden temperature drop experienced by gases from the headspace, the fall of CO_2 partial pressure above the champagne surface linked with bottle uncorking leads to a huge consequence concerning the thermodynamic equilibrium of CO_2-dissolved molecules. Since the partial pressure of CO_2 falls above the champagne surface, the CO_2 dissolved in champagne is not in equilibrium any longer with its partial pressure in the vapor phase. Champagne enters a metastable state, *i.e.*, it contains CO_2 molecules in excess in comparison with what Henry's law states. To recover a new stable thermodynamic state corresponding to the partial pressure of CO_2 molecules in the atmosphere (about only 3.5×10^{-4} atm), almost all the carbon dioxide molecules dissolved in the champagne must escape. The champagne becomes supersaturated with CO_2. Before proceeding further, it is important to define the supersaturating ratio, used for quantifying CO_2 molecules in excess in a carbonated liquid. The supersaturating ratio S is defined as follows:[7]

$$S = \frac{c_L}{c_0} - 1 \qquad (9)$$

where c_L is the concentration of CO_2 in the liquid bulk, and c_0 is the equilibrium concentration of CO_2 corresponding to a partial pressure of gaseous CO_2 of 1 atm.

As soon as $S > 0$, a supersaturated liquid enters a metastable state and must degas to recover a supersaturating ratio equal to zero. In the case of Champagne wines, just after uncorking the bottle, c_L is the equilibrium concentration of CO_2 in the liquid bulk corresponding to a partial pressure of CO_2 of about 5 atm. Because there is a strict proportionality between the concentration of dissolved CO_2 and its partial pressure in the vapor phase (as expressed by Henry's law), $c_L/c_0 \approx 5$. Therefore, just after uncorking the bottle, the supersaturating ratio of champagne is approximately $S \approx 4$, and champagne must degas. Actually, there are two mechanisms for gas loss: (i) losses due to diffusion through the surface of the liquid (invisible to the naked eye), and (ii) losses due to bubbling (the so-called effervescence process). But, how and where do all these bubbles form, or *nucleate*?

3. The bubble nucleation process

3.1. The critical radius required for bubble nucleation

Generally speaking, carbonated beverages are weakly supersaturated with CO_2-dissolved gas molecules. In weakly supersaturated liquids such as champagne and sparkling wines, bubbles do not just pop into existence *ex nihilo*. Actually, to cluster into the form of bubbles, CO_2-dissolved gas molecules must cluster together and push their way through the liquid molecules that are held together by Van der Waals attractive forces. Bubble formation is therefore limited by an energy barrier (for a complete review see the paper by Lugli and Zerbetto[8]). This is the reason why in weakly supersaturated liquids, bubble formation and growing require preexisting gas cavities with radii of curvature large enough to overcome the nucleation energy barrier and grow freely.[9,10] This critical radius, denoted r^*, can easily be accessed by using standard thermodynamic arguments, or by using simple arguments based on classical diffusion principles. The critical radius r^* of gas pockets required to enable bubble production in a carbonated beverage is expressed as follows (see ref. 11 and references therein),

$$r^* \approx \frac{2\gamma}{P_0 S} \qquad (10)$$

where γ is the surface tension of the liquid medium (in the order of 50 mN m^{-1} in champagne and sparkling wines[5]), and P_0 is the atmospheric pressure ($P_0 \approx 10^5$ N m^{-2}). At the opening of a champagne bottle, because $S \approx 4$, the critical radius required to enable bubble nucleation is in the order of 0.25 μm.

Jones *et al.* made a classification of the broad range of nucleation likely to be encountered in liquids supersaturated with dissolved gas molecules.[9] Bubble formation from preexisting gas cavities larger than the critical size is referred to as non-classical heterogeneous bubble nucleation (type IV bubble nucleation, following their nomenclature). Generally speaking, effervescence in a glass of champagne or sparkling wine may have two distinct origins. It can be "natural" or "artificial".

3.2. "Natural" bubble nucleation

Natural effervescence is related to the bubbling process from a glass which has not experienced any specific surface treatment. Closer inspection of such glasses poured with champagne and sparkling wines revealed that most of the bubble nucleation sites were found to be located on preexisting gas cavities trapped inside hollow and roughly cylindrical cellulose-fibre-made structures on the order of 100 μm long with a cavity mouth of several micrometres (see Fig. 6).[11–14] The hollow cavity (a kind of tiny channel within the fibres) where a gas pocket is trapped during the pouring process is called the *lumen*. It can be clearly noticed from Fig. 6 that the radii of curvature of gas pockets trapped inside the fibre's lumen are

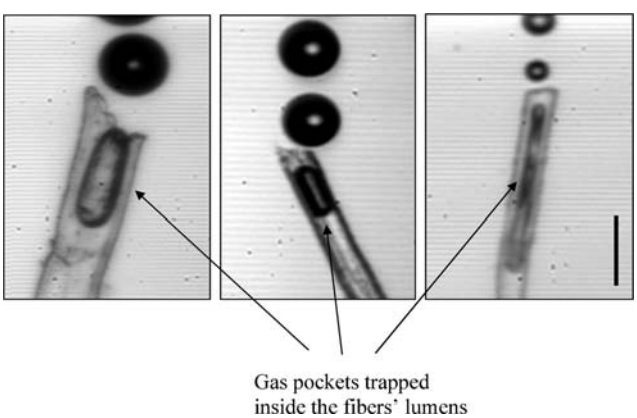

Fig. 6 Three typical cellulose fibres adsorbed on the wall of a glass poured with champagne; the gas pockets trapped inside the fibres' lumens and responsible for bubble formation clearly appear (bar = 50 μm). (Photographs by Gérard Liger-Belair.)

much higher than the above-mentioned critical radius r^*. Fibres probably adhere on the flute wall due to electrostatic forces (especially if the glass or the flute is vigorously wiped by a towel). Natural effervescence may also arise from gas pockets trapped inside tartrate crystals precipitated on the glass wall and resulting from the evaporation process after rinsing the glass with tap water. Therefore, there is a substantial variation concerning the ''natural'' effervescence between flutes depending on how the flute was cleaned and how and where it was left before serving.

The mechanism of bubble release from a fibre's lumen has already been described in recent papers.[14–17] In short, after opening a bottle of champagne or sparkling wine, the thermodynamic equilibrium of CO_2 molecules dissolved in the liquid medium is broken. CO_2-dissolved molecules become in excess in comparison with what the liquid medium can withstand. Therefore, CO_2 molecules will escape from the liquid medium through every available gas/liquid interface to reach a vapor phase. Actually, once the sparkling beverage is poured into a glass, the tiny air pockets trapped inside the collection of fibres adsorbed on the glass wall offer gas/liquid interfaces to CO_2 dissolved molecules, which cross the interface toward the gas pockets. In turn, the gas pockets grow inside the fibres' lumens. When a gas pocket reaches the tip of a fibre, a bubble is ejected, but a portion of the gas pocket remains trapped inside the fibre's lumen, shrinks back to its initial position, and the cycle starts again until bubble production stops through lack of dissolved gas molecules (see the very typical time sequence displayed in Fig. 7). The fibre displayed in Fig. 7 is a sort of textbook case, the behaviour of which was recently understood and modelled.[14,16]

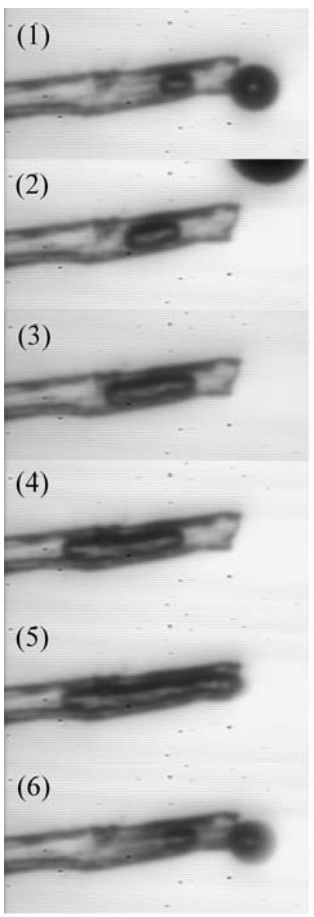

Fig. 7 Time-sequence illustrating one period of the cycle of bubble production from the lumen of a typical hollow cellulose fibre adsorbed on the wall of a glass poured with champagne; from frame 1 to frame 5, the time interval between successive frames is about 200 ms, but from frame 5 to frame 6, the time interval is only 1 ms (bar = 50 μm). (Photographs by Cédric Voisin and Gérard Liger-Belair.)

3.3. Entrapping an air pocket within a fibre

Cellulose fibres are in the form of hollow tubes of several hundreds of micrometres long and with a cavity mouth of several micrometres wide. The fibre wall section consists of densely packed cellulose micro fibrils, with a preferential orientation along the fibre axis. Cellulose micro fibrils consist of glucose units bounded in a β-conformation favouring straight polymer chains. The different structural levels of a cellulose fibre are presented in Fig. 8. For a current review on the molecular and supramolecular structures of cellulose, see the article by O'Sullivan[18] and references therein.

From the physics point of view, cellulose fibres can indeed be considered as tiny roughly cylindrical capillary tubes of radius r and length h. Consequently, a wetting liquid placed into contact with this highly hydrophilic material penetrates it by capillary action. Actually, in capillaries with radii much smaller than the capillary length, gravity may be neglected. Therefore, with η being the viscosity of the liquid phase, γ being the surface tension of the liquid, z being the distance of

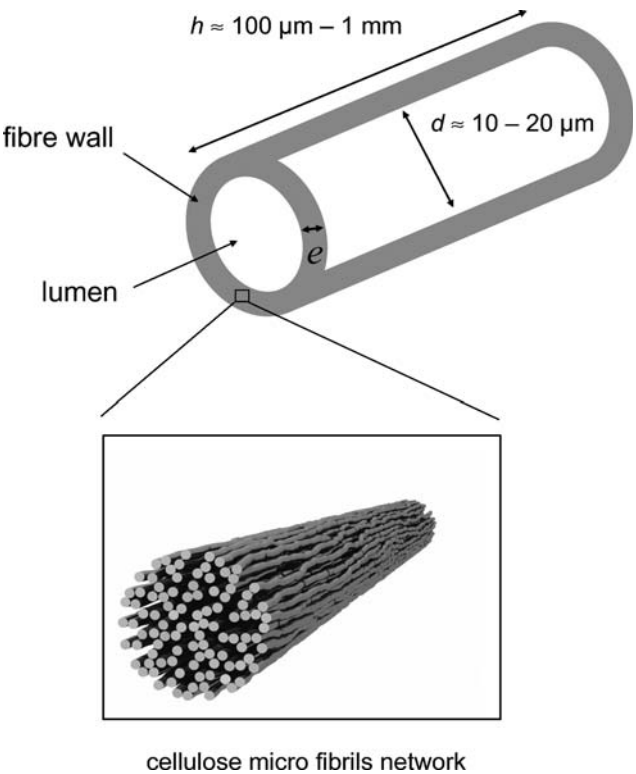

Fig. 8 The different structural levels of a typical cellulose fibre; the fibre wall consists of closely packed cellulose micro fibrils oriented mainly in the direction of the fibre.[18]

penetration at time t, and θ the effective contact angle between the liquid and the capillary wall, the overall balance of forces on the liquid in the capillary may be expressed as,

$$\rho\left[z\frac{d^2z}{dt^2}+\left(\frac{dz}{dt}\right)^2\right]=\frac{2\gamma\cos\theta}{r}-\frac{8\eta z}{r^2}\frac{dz}{dt} \quad (11)$$

The left-hand side of eqn (11) is related to the liquid inertia, whereas both terms in the right-hand side are related to capillarity (the driving force), and viscous resistance, respectively. Under steady state conditions, capillarity is balanced by the viscous drag of the liquid, and the famous Lucas–Washburn equation can be derived:[19,20]

$$z^2=\frac{r\gamma\cos\theta}{2\eta}t \quad (12)$$

Let's imagine a liquid edge spreading with a velocity v along a solid surface where cellulose fibres are adsorbed. This is basically what happens when you fill a glass with a liquid. Actually, a liquid edge progressively advances along the vertical glass wall at a velocity v in the order of several cm s^{-1}. As soon as the wetting liquid gets in touch with the fibre, some liquid progressively penetrates and fills the fibre's lumen by capillary rise. Finally, a gas pocket may be trapped within the fibre if the time τ taken by the liquid to completely fill the lumen by capillary action is greater than the characteristic time T taken by the liquid edge to completely submerge the fibre inside the liquid (see the scheme displayed in Fig. 9).

By retrieving eqn (12) with the characteristic fibre's parameters defined in Fig. 9, the characteristic time required to completely fill the fibre's lumen by capillary action may be expressed as,

$$\tau=\frac{2\eta h^2}{r\gamma\cos\theta} \quad (13)$$

Considering a fibre with a length h, inclined by an angle α with regard to the liquid edge advancing over it at a velocity v, leads to the following time required for the fibre to be completely submerged:

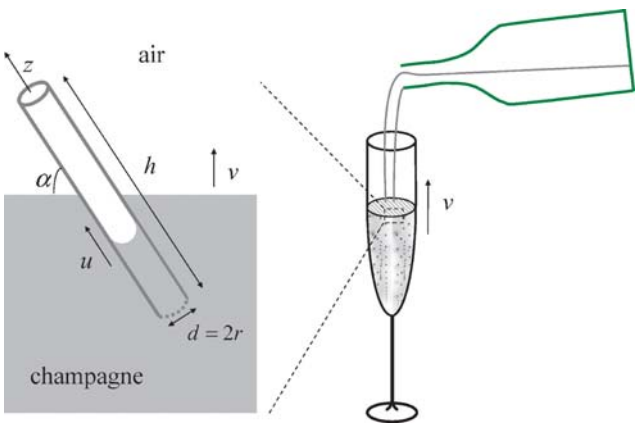

Fig. 9 From the physics point of view, a fibre may be seen as a tiny capillary tube which gets invaded by a wetting liquid placed into contact with one of the fibre's tip; v is the velocity of the liquid edge advancing over the fibre, and u is the velocity at which the meniscus advances inside the fibre's lumen by capillary action.

$$T=\frac{h\sin\alpha}{v} \quad (14)$$

The condition of gas entrapment inside the fibre therefore is expressed as $\tau > T$, *i.e.*,

$$\frac{2\eta h^2}{r\gamma\cos\theta}>\frac{h\sin\alpha}{v} \quad (15)$$

Because cellulose is a highly hydrophilic material, the contact angle of an aqueous liquid on it is relatively small (about 30° with pure water). Consequently, $\cos\theta \approx 1$. Finally, the condition of entrapment may be rewritten as follows,

$$\frac{h}{r\sin\alpha}>\frac{\gamma}{2\eta v} \quad (16)$$

with the geometric parameters of the cellulose fibre lying on the left-hand side of eqn (16), and the liquid parameters lying on the right-hand side of eqn (16).

The entrapment of an air pocket inside the lumen of a fibre during the filling of a glass is therefore favoured by the following conditions, depending on both fibre and liquid parameters: (i) as elongated fibres as possible (h long), (ii) small lumen radii r, (iii) fibres as horizontal as possible with regard to the liquid edge (*i.e.*, $\sin\alpha$ small), (iv) liquids with a small surface tension γ, (v) and a high viscosity η, and finally (vi) a high velocity for the liquid edge advancing along the glass wall. It is worth noting that both conditions (iv) and (v) imply that hydroalcoholic carbonated beverages are more favourable than fizzy waters to entrap air pockets inside cellulose fibres during the pouring process. Actually, the surface tension of champagne and beer is in the order of 50 mN m^{-1} (*i.e.*, about 20 mN m^{-1} less than the surface tension of pure water), and their dynamic viscosity is about 50% higher than that of pure water.

3.4. Modelling the repetitive bubble nucleation from a cellulose fibre

As seen in Fig. 7, the whole process leading to the production of a bubble from a cellulose fibre's tip can be coarsely divided in two main steps: (i) the growth of the gas pocket trapped inside the fibre's lumen (from frame 1 to frame 5), and (ii) the bubble detachment as the gas pocket reaches the fibre's tip (from frame 5 to frame 6). Actually, it is clear from the numerous close-up time sequences taken with the high-speed video camera that the time scale of the bubble detachment is always very small ($\approx$1 ms) compared with the relatively slow growth of the gas pocket (several tens to several hundreds of ms). Therefore, the whole cycle of bubble production seems to be largely governed by the growth of the gas pocket trapped inside the fibre's lumen. This tiny gas pocket was modelled as a slug-bubble growing trapped inside an ideal cylindrical micro channel and being fed with CO_2-dissolved molecules diffusing (i) directly from both ends of the gas pocket, and (ii) through the fibre wall, which consists of closely packed cellulose micro fibrils oriented mainly in the direction of the fibre.[21] A scheme is displayed in Fig. 10, where the geometrical parameters of the tiny gas pocket growing by diffusion are defined.

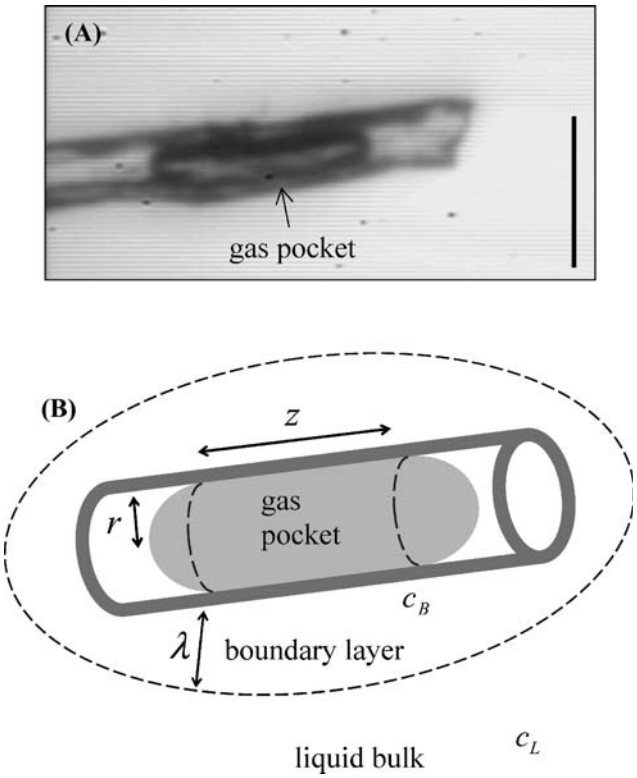

Fig. 10 Real gas pocket trapped within the lumen of a cellulose fibre acting as a bubble nucleation site in a glass poured with champagne (A), modelled as a slug-bubble trapped inside an ideal cylindrical micro channel and being fed with CO_2-dissolved molecules diffusing, (i) directly from the liquid bulk through both ends of the gas pocket, and (ii) through the wall of the micro channel (B) (bar = 50 μm).

Taking into account the diffusion of CO_2-dissolved molecules from the liquid bulk to the gas pocket *via* the two ways defined above, the growth of this gas pocket with time t was linked with both liquid and fibre parameters as follows:[14]

$$\begin{cases} z(t) \approx (z_0 + A\tau)\exp(t/\tau) - A\tau \\ \text{with } \tau = \dfrac{(P + 2\gamma/r)r\lambda}{2\Re\theta D_\perp \Delta c}, \text{ and } A = \dfrac{4\Re\theta D_0 \Delta c}{(P + 2\gamma/r)\lambda} \end{cases} \quad (17)$$

where z is the length of the gas pocket, z_0 is the initial length of the gas pocket before it starts its growth through the lumen, at each cycle of bubble production (see for example frame 1 and frame 6 in Fig. 7), P is the ambient pressure, D_0 is the diffusion coefficient of CO_2-dissolved molecules in the liquid bulk, $D_\perp$ is the diffusion coefficient of CO_2-dissolved molecules through the fibre wall (and therefore perpendicular to the cellulose micro fibrils), $\Delta c = c_L - c_B = c_L - k_H P_B = c_L - k_H(P_0 + 2\gamma/r)$ is the difference in CO_2-dissolved concentrations between the liquid bulk and the close vicinity of the gas pocket surface in equilibrium with the gaseous CO_2 in the gas pocket, and λ is the boundary layer thickness where a linear gradient of CO_2-dissolved concentration is assumed.

In a previous work, the transversal diffusion coefficient $D_\perp$ of CO_2 molecules through the fibre wall was approached and properly bounded by $D_\perp/D_0 \approx 0.1$ and $D_\perp/D_0 \approx 0.3$.[21] For modelling purposes, an intermediate value of about $D_\perp \approx 0.2D_0$ was proposed and will be used hereafter.[21] The whole cycle of bubble production being largely governed by the growth of the gas pocket trapped inside the fibre's lumen, the period of bubble formation from a single cellulose fibre is therefore equal to the total time T required by the tiny gas pocket to grow from its initial length, denoted z_0, to its final length, denoted z_f, as it reaches the fibre's tip (see frame 5 in Fig. 7). By retrieving eqn (17), it is therefore possible to access the frequency of bubble formation f from a single fibre as follows:

$$f \approx \frac{1}{T} \approx \frac{2\Re\theta D_\perp \Delta c}{r\lambda(P_0 + 2\gamma/r)\ln[(z_f + 10r)/(z_0 + 10r)]} \quad (18)$$

To go further on with the dependence of the bubbling frequency on both liquid and fibre parameters, we can replace in eqn (18) the diffusion coefficient D_0 by its theoretical expression approached through the well-known Stokes–Einstein equation ($D_0 \approx k_B\theta/6\pi\eta d$), k_B being the Boltzmann constant (1.38×10^{-23} J K^{-1}), and d being the characteristic size of the CO_2 molecule's hydrodynamic radius ($d \approx 10^{-10}$ m). By replacing in eqn (18) each parameter by its theoretical expression and each constant by its numerical value, the variation of the bubbling frequency as a function of the various pertinent parameters involved may be rewritten as follows (in the MKSA system):

$$f \approx 2.4 \times 10^{-14} \frac{\theta^2[c_L - k_H(P + 2\gamma/r)]}{\eta r(P + 2\gamma/r)\lambda \ln[(z_f + 10r)/(z_0 + 10r)]} \quad (19)$$

The boundary layer thickness λ was indirectly approached in a recent paper and found to be in the order of 20 μm.[14] Finally, let us apply eqn (19) to the standard textbook case fibre displayed in Fig. 7 and modelled in Fig. 10 (*i.e.*, $r \approx 5$ μm, $z_0 \approx 20$ μm and $z_f \approx 100$ μm). Eqn (19) may therefore be rewritten as follows, by replacing the fibre's parameters r, z_0, z_f and λ by their numerical values:

$$f \approx 5.2 \times 10^{-8} \frac{\theta^2[c_L - k_H(P + 0.2)]}{\eta(P + 0.2)} \quad (20)$$

In the latter expression, c_L is expressed in g L^{-1}, k_H in g L^{-1} atm^{-1}, P in atm, and η in kg m^{-1} s^{-1}, to fit the standards used in enology.

We will discuss the relative influence of the following parameters on the average bubbling frequency: (i) the concentration c_L of CO_2-dissolved molecules, (ii) the liquid temperature θ, and (iii) the ambient pressure P.

(i) Following eqn (20), every other parameter being constant, the dependence of the theoretical average bubbling frequency f on the CO_2-dissolved concentration c_L is in the form $f = ac_L - b$. By use of a high-speed video camera fitted with a microscope objective, a few cellulose fibres acting as bubble nucleation sites on the wall of a glass poured with champagne were followed over time during the whole gas discharging process (which may last up to several hours). This method is developed in minute details in ref. 16. The dependence of the experimental bubbling frequency f_{exp} with c_L was found to follow a linear-like c_L dependence, as expected from the model developed above. Therefore, the frequency of bubble formation from a given nucleation site is found to progressively decrease with time, because the concentration c_L

of CO_2-dissolved molecules progressively decreases as CO_2 continuously desorbs from the champagne matrix. Furthermore, it is worth noting that the bubbling frequency of a given nucleation site vanishes (*i.e.*, the bubble release ceases, $f \rightarrow 0$ bubble s^{-1}), although the CO_2-dissolved concentration c_L remains higher than a critical value, as shown in ref. 16. Actually, following both Laplace's and Henry's laws, the curvature r of the CO_2 pocket trapped inside the fibre's lumen induces in the close vicinity of the trapped CO_2 pocket a concentration c_B of CO_2-dissolved molecules in the order of $k_H(P_0 + 2\gamma/r)$. Consequently, as soon as the concentration of CO_2-dissolved in the liquid bulk reaches a critical value $c^*_L = c_B \approx k_H(P_0 + 2\gamma/r)$, the diffusion toward the gas pocket ceases and the given nucleation site stops releasing bubbles (simply because Δc, the driving force of diffusion, vanishes as $c_L \approx c^*_L$). Let us apply the latter condition to the characteristic radius of a cellulose fibre ($r \approx 5$ μm). At 10 °C, the critical concentration c^*_L below which bubble release becomes impossible is therefore:

$$\begin{aligned} c^*_L &\approx k_H(P_0 + 2\gamma/r) \\ &\approx 2.07 \times 10^{-5}(10^5 + 2 \times 5 \times 10^{-2}/5 \times 10^{-6}) \\ &\approx 2.5 \text{ g L}^{-1} \end{aligned} \quad (21)$$

(ii) The dependence of the bubbling frequency on the liquid temperature is much more difficult to test experimentally in real consuming conditions. Actually, we needed time to decrease or increase the liquid temperature, and we found no satisfying possibility of modifying the liquid temperature without significantly losing CO_2-dissolved molecules which continuously desorb from the supersaturated liquid matrix due to diffusion through the liquid surface and due to bubbling from the numerous nucleation sites found in the flute. We will nevertheless discuss the theoretical influence of the liquid temperature by retrieving eqn (20). In eqn (20), the temperature directly appears as θ^2, but the Henry's law constant k_H, as well as the champagne dynamic viscosity η are strongly temperature-dependent.[22] Increasing the liquid temperature by 10 K (let us say from 278 to 288 K, which is approximately the range of champagne tasting temperatures) increases the theoretical bubbling frequency by about 50%. For the fibre displayed in Fig. 7 ($r \approx 5$ μm, and $z_0 \approx 20$ μm and $z_f \approx 100$ μm) and with $c_L \approx 12$ g L^{-1}, the theoretical temperature dependence of the bubbling frequency is displayed in Fig. 11.

(iii) Increasing or decreasing the ambient pressure P also significantly modifies the corresponding average bubbling frequency f. For the fibre displayed in Fig. 7 ($r \approx 5$ μm, $z_0 \approx 20$ μm and $z_f \approx 100$ μm) and with $c_L \approx 12$ g L^{-1}, the theoretical pressure dependence of the bubbling frequency is displayed in Fig. 12. Reducing the ambient pressure to only 0.3 atm (on the top of Mount Everest for example) would increase the average bubbling frequency by a factor of almost 3. This is basically the same phenomenon which is responsible for gas embolism in divers who have breathed high-pressure air under water if they resurface too quickly. Inversely, increasing the ambient pressure to 2 atm decreases the average bubbling frequency by a factor of about 2 compared to that at sea level.

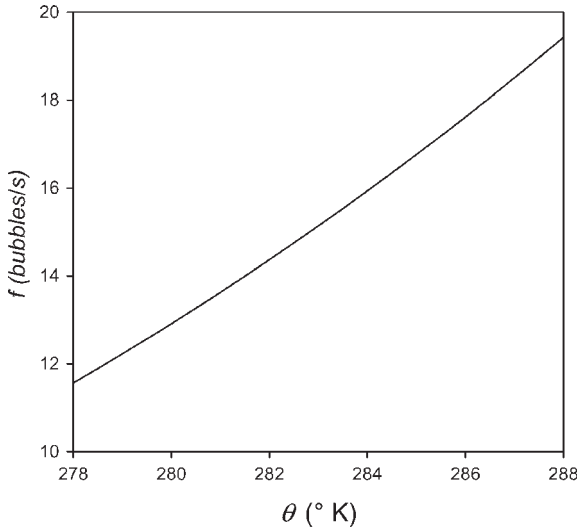

Fig. 11 Theoretical dependence of the bubbling frequency f on temperature θ, as expected from the model displayed in eqn (20), in the range of usual champagne-tasting temperatures (from 5 to 15 °C), and for the textbook case fibre displayed in Fig. 7.

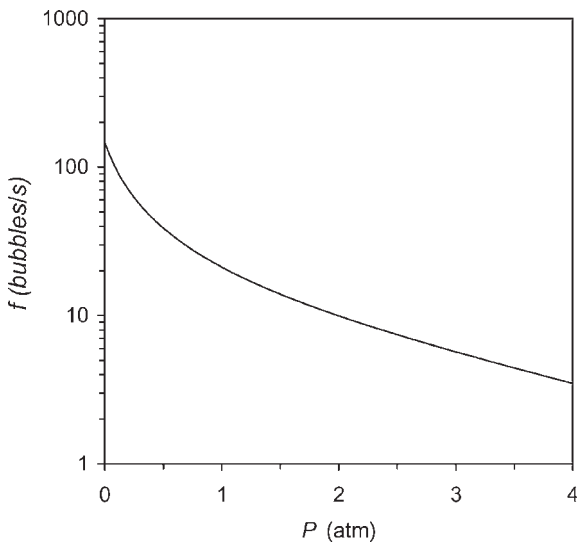

Fig. 12 Theoretical dependence of the bubbling frequency f on the ambient pressure P (at 20 °C), as expected from the model displayed in eqn (20) for the textbook case fibre displayed in Fig. 7.

3.5. Evidence for bubbling instabilities

The regular and clockwork release of bubbles from a cellulose fibre is indeed the most common and usual way of blowing bubbles, but cellulose fibres were recently found to experience other various and sometimes very complex rhythmical bubbling regimes.[23,24] After pouring champagne into a flute, thorough examination (even by the naked eye) of the bubble trains rising toward the liquid surface recently revealed a curious and quite unexpected phenomenon. As time proceeds, during the gas discharging process from the liquid matrix, some of the bubble trains showed abrupt transitions during

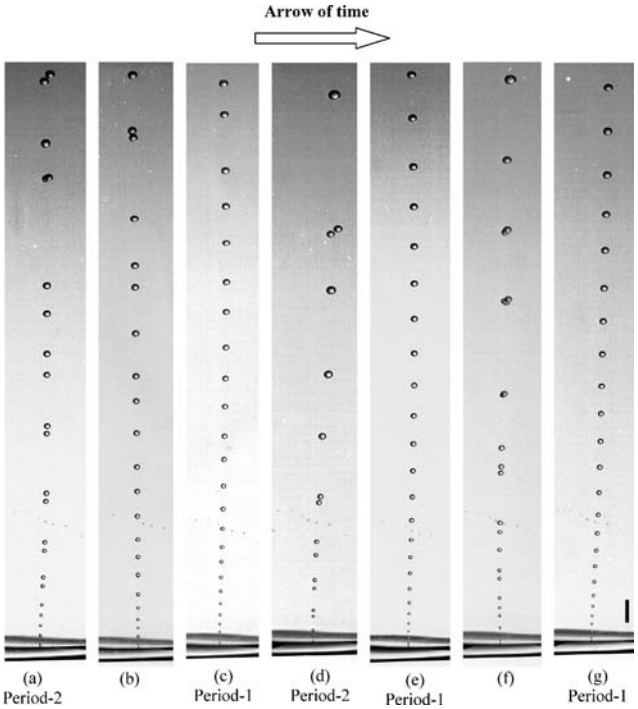

Fig. 13 Time sequence (from left to right) showing a bubble nucleation site at the bottom of a flute poured with champagne blowing bubbles through different and well-established bubbling regimes (bar = 1 mm). (Photographs by Gérard Liger-Belair.)

the repetitive and rhythmical production of bubbles. Visually speaking, the macroscopic pertinent parameter which is characteristic from the successive bubbling regimes is the interbubble distance between the successive bubbles of a given bubble train. In Fig. 13, micrographs of a bubble train in its successive rhythmical bubbling regimes while degassing are displayed. The duration of a given bubbling regime may vary from a few seconds to several minutes. In frame (a), bubbles are seen to be generated from a period-2 bubbling regime which is characterized by the fact that two successive bubbles rise in pairs. Then, the bubbling regime suddenly changes, and a multiperiodic bubbling regime arises which is displayed in frame (b). Later, in frame (c), clockwork bubbling in period-1 occurs where the distance between two successive bubbles increases monotonically as they rise, and so on. This nucleation site experienced other various bubbling regimes during its

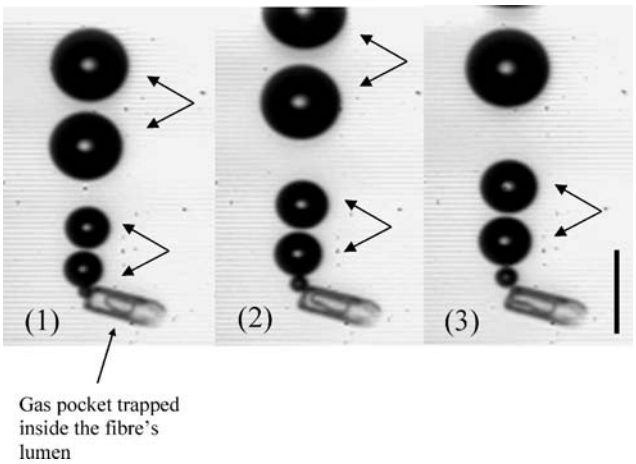

Fig. 14 Close-up time sequence illustrating a tiny cellulose fibre acting as a bubble nucleation site in its period-2 bubbling regime (*i.e.*, bubbles are blown by pairs); the time interval between two successive frames is 40 ms (bar = 50 μm). (Photographs by Gérard Liger-Belair.)

life, until it finally ended in a clockwork period-1 bubbling regime presented in frame (g).

Such a curious and unexpected observation raises the following question: what is/are the mechanism(s) responsible for the transitions between the different bubbling regimes? To better identify the fine mechanisms behind this rhythmical production of bubbles from a few nucleation sites, some of them experiencing bubbling transitions were filmed *in situ* by use of a high-speed digital video camera. Two time sequences are displayed in Fig. 14 and 15, where bubbles are blown in a period-2 and in a very erratic way, respectively. The lumen of the cellulose fibre displayed in Fig. 14 presents only one gas pocket, whereas the fibre's lumen displayed in Fig. 15 clearly shows two gas pockets periodically touching and connecting themselves through a tiny gas bridge (see frames 3 and 4 of Fig. 15). The micrometric gas bridge connecting the two gas pockets and disturbing the overall production of bubbles is enlarged in Fig. 16. This tiny gas bridge is a likely source of bubbling instabilities. Recently, a model was built which takes into account the coupling between the bubbling frequency and the frequency of the single gas pocket which oscillates while trapped inside the fibre's lumen (as in Fig. 14, for example). The previously published data showed a general rule concerning bubbling instabilities arising from some fibres

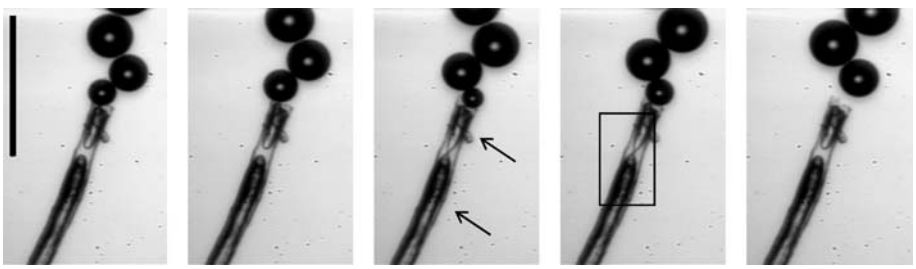

Fig. 15 Two gas pockets are interacting in the lumen of this cellulose fibre, thus disturbing the periodicity of the bubbling regime; the black arrows point to the various gas pockets interacting; the time interval between two successive frames is 10 ms (bar = 100 μm). (Photographs by Gérard Liger-Belair.)

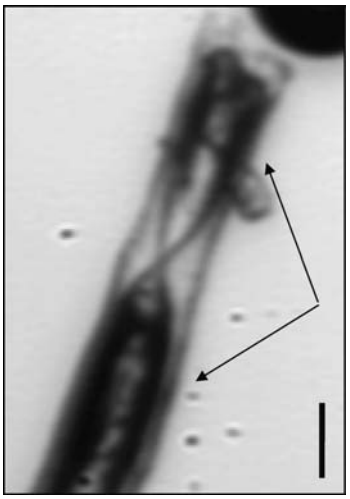

Fig. 16 Detail of the cellulose fibre displayed in Fig. 15, which clearly shows the establishment of a micrometric gas bridge between the two gas pockets trapped inside the fibre's lumen (bar = 10 μm). (Photograph by Gérard Liger-Belair.)

presenting just one trapped gas pocket. In this previous paper, the successive rhythmical bubbling regimes followed the so-called "period-adding scenario".[23] Nevertheless, this previously published scenario does not fit the various ways of blowing bubbles from more complex cellulose fibres able to entrap numerous gas pockets as shown in Fig. 15. Numerous fibres, such as those shown in the present paper, presented a sequence of various bubbling instabilities which is not reproduced by our previous model. A huge collection of successive rhythmical bubbling regimes has already been observed, and the highest recorded periodicity was observed for a fibre presenting a period-12 bubbling regime.[24] At the moment, we cannot find any general rule with fibres presenting numerous gas pockets interacting together, but the close up observation and the discovery of the multiple gas pockets interacting together is considered as a step toward a deeper understanding of the successive rhythmical bubbling regimes arising from complex fibres. The huge diversity in our observations, in terms of the various successive bubbling regimes seems to be directly linked with the "natural" variability of cellulose fibres (in terms of size, lumen diameter, inner wall properties...).

3.6. A word about *fliers*

Some of the particles acting as bubble nucleation sites (most of them including cellulose fibres) may detach from the glass wall to finally get completely immersed in the champagne bulk. Particles detached from the glass wall are nevertheless still active (in terms of bubbling capacity) provided that a gas pocket with a radius of curvature larger than the critical radius has been trapped inside them. Those particles immersed in the champagne bulk produce easily-recognizable bubble trains, which seem to dance erratically inside the glass during champagne tasting. Those particles in suspension in champagne glasses are called *fliers* (due to their often complex and circling trajectories in the champagne bulk). Fliers are indeed a significant source of bubbles in glasses poured with champagne. The photograph of a typical flute poured with champagne displayed in Fig. 1a shows a detail in Fig. 1b, where some fliers are recognizable. Fliers undoubtedly catch the eyes of champagne-tasters, who also often are fine observers. The dynamics of fliers was recently investigated by use of long exposure time photography and laser tomography techniques.[25] By use of long exposure time photography, the trajectories of bubbles released by fliers were found to leave very elegant and characteristic "prints" as they crossed a section of champagne illuminated with a 1 mm-thick laser sheet (see for example the tomography displayed in Fig. 17). Because the flier immersed in the champagne bulk is constantly moving, trajectories of bubbles released during the 1 s exposure-time photography do not superimpose on each other. Therefore, the print left by a flier which crosses the laser sheet during the exposure time of the digital camera is a typical multiple filaments structure, each filament materializing the trajectory of a single rising bubble.

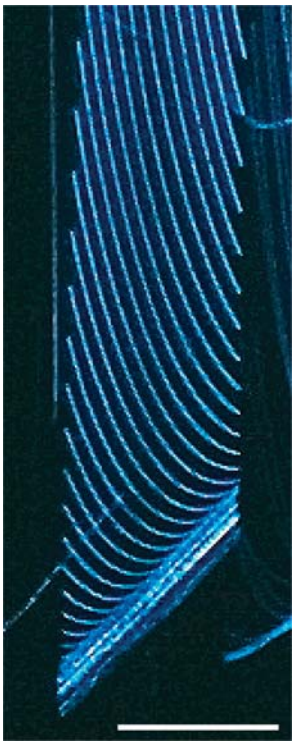

Fig. 17 Characteristic print left by the bubbles released from a flier along its 1 s-path through a 2 mm-thick laser sheet which crosses a flute poured with champagne; under laser illumination, the print left by the flier during the 1 s-exposure time of a digital camera is a typical multiple filaments structure, each filament materializing the trajectory of a single bubble released from the flier (bar = 5 mm). (Photograph by G. Liger-Belair, F. Beaumont and G. Polidori.)

3.7. "Artificial" bubble nucleation

Artificial effervescence is related to bubbles nucleated from glasses with imperfections done intentionally by the glassmaker to promote or to eventually replace a deficit of "natural" nucleation sites. Actually, it has been known for decades that bubbles may arise from microscratches on the glass wall.[26,27] Those microscratches are geometrically able to

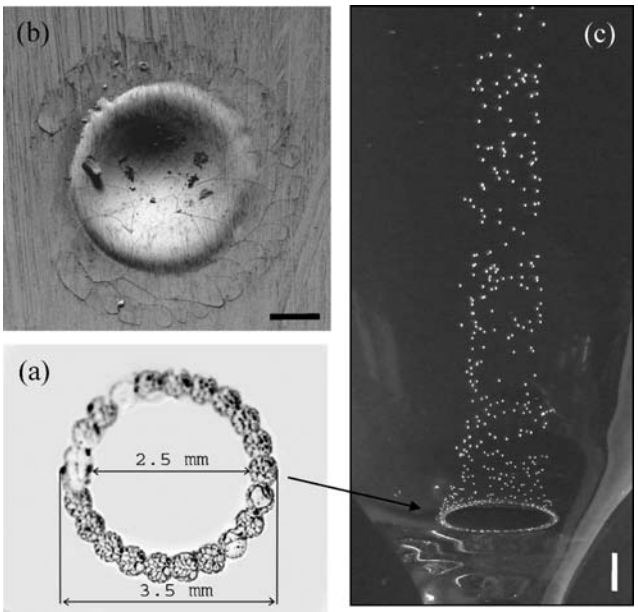

Fig. 18 At the bottom of this flute, on its axis of symmetry, the glassmaker has engraved a small ring (done with adjoining laser beam impacts) (a); single laser beam impact as viewed through a scanning electron microscope (bar = 100 μm) (b); effervescence in this flute is promoted from these "artificial" micro scratches in the form of a characteristic and easily recognizable vertical bubbles column rising on its axis of symmetry (bar = 1 mm) (Photographs by G. Polidori and F. Beaumont) (c).

trap tiny air pockets when champagne is poured into the glass (as cellulose fibres do). Those microscratches on a glass can be done by essentially two techniques: sandblast or laser engraving. Nevertheless, effervescence produced from scratches intentionally done by the glassmaker does not resemble that arising from tiny individual cellulose fibres. A rendering of such micro scratches releasing bubbles at the bottom of a champagne flute is displayed in Fig. 18. It is worth noting that the repetitive bubbling process arising from artificial bubble nucleation is much more vigorous and chaotic than the bubbling process from tiny cellulose fibres. Glasses engraved at their bottom are thus indeed easily recognizable, with a characteristic bubble column rising on their axis of symmetry.[28] Effervescence promoted by engraved glasses is indeed visually quite different than that naturally promoted by cellulose fibres, but the difference is also suspected to go far beyond the solely aesthetical (and rather subjective) point of view. Differences are strongly suspected concerning the kinetics of CO_2 and flavour release throughout champagne tasting (see section 4.3).

4. Bubble growth, bubble rise, and mixing flow patterns found in champagne glasses

4.1. Bubble growth and rise

After being born in micrometric gas pockets trapped inside impurities of the glass wall, bubbles rise toward the liquid surface due to their own buoyancy. While rising, they continue to grow in size by continuously absorbing carbon dioxide

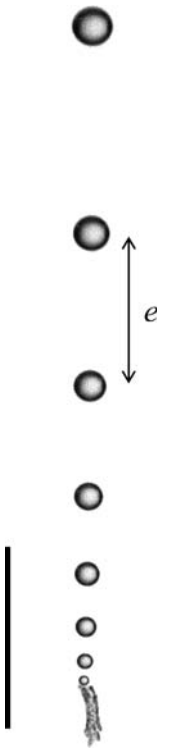

Fig. 19 A characteristic bubble train promoted by the repetitive bubble formation process from a single cellulose fibre; bubbles are clearly seen growing during their way up (bar = 1 mm). (Photograph by Gérard Liger-Belair.)

molecules dissolved in the liquid "matrix", as is clearly illustrated in the photograph displayed in Fig. 19. Growing bubbles thus continuously accelerate along their way through the champagne. This continuous acceleration is also betrayed, in high-speed photographs, by the continuously increasing spacing e between the successive bubbles of a given bubble train (see Fig. 19 for example).

The clockwork repetitive bubble production from nucleation sites was used to develop a simple set-up which consists of the association of a photo camera with a stroboscopic light to follow the motion of bubbles.[12] It was found that the bubble radius R of bubbles increases at a constant rate $k = dR/dt$, as they rise toward the liquid surface. Thus,

$$R(t) = R_0 + kt \qquad (22)$$

where R_0 is the bubble radius as it detaches from the nucleation site. R_0 is of the same order of magnitude as the radius of the mouth of the cellulose fibre which acts as the nucleation site, *i.e.*, around 5 to 10 μm.[11–13]

Three minutes after pouring, experiments conducted with champagne and sparkling wines led to growth rates k ranging between approximately 350 and 400 μm s^{-1}, at 20 °C.[11] Experiments were also performed with the growth rates of bubbles rising in beer glasses. In beer, three minutes after pouring, bubble growth rates were found to lay around 100–150 μm s^{-1}, *i.e.*, about three times less than those in champagne and sparkling wines.[12]

The growth rate k of bubbles rising in champagne and beer was also modelled and linked with some physicochemical properties of liquids as follows (in the MKSA system):[12]

$$k = \frac{\mathrm{d}R}{\mathrm{d}t} \approx 0.63 \frac{\Re\theta}{P_\mathrm{B}} D_0^{2/3} \left(\frac{2\alpha\rho g}{9\eta}\right)^{1/3} \Delta c \qquad (23)$$

where θ is the liquid temperature, $\Re$ is the ideal gas constant, P_B is the pressure inside the rising bubble, D_0 is the diffusion coefficient of CO_2 molecules through the liquid bulk, ρ and η are respectively the liquid density and viscosity, g is the acceleration due to gravity, α is a numerical pre-factor close to 0.7 for champagne and sparkling wine bubbles,[11] h is the distance travelled by the bubble from its nucleation site, and Δc (the driving force responsible for the diffusion of CO_2 into the rising bubble) is the difference in dissolved-CO_2 concentrations between the liquid bulk and the close vicinity of the bubble surface which is in equilibrium with the gaseous CO_2 in the rising bubble (see Fig. 20).

Strictly speaking, the pressure P_B inside the rising bubble is the sum of three terms: (i) the atmospheric pressure P_0, (ii) the hydrostatic pressure $\rho g H$, and (iii) the Laplace pressure $2\gamma/R$, originating from the bubble's curvature. H is the depth at which the bubble rises, and γ is the surface tension of the liquid medium. However, with H varying from several millimetres to several centimetres, the surface tension of champagne being in the order of 50 mN m^{-1},[5] and bubbles' radii varying from several tens to several hundreds of micrometres, the contribution of both hydrostatic and Laplace pressures are clearly negligible in terms of the atmospheric pressure P_0.

Let us test the applicability of eqn (23) in the case of rising and expanding champagne bubbles at 20 °C. By using known values of ρ and η in champagne,[12] $\alpha = 0.7$, $D_0 \approx 1.4 \times 10^{-9}$ m^2 s^{-1} (as measured by nuclear magnetic resonance[29]), and the difference in CO_2 concentrations between the liquid bulk and the close vicinity of the bubble surface $\Delta c \approx 10$ g $L^{-1} \approx 227$ mol m^{-3}, one finds,

$$k \approx 0.63 \times \frac{8.31 \times 293}{10^5} \times (1.4 \times 10^{-9})^{2/3} \times \left[\frac{2 \times 0.7 \times 10^3 \times 9.8}{9 \times 1.5 \times 10^{-3}}\right]^{1/3} \times 193 \approx 430\ \mu\ \mathrm{m\ s^{-1}}$$

which is in very good accordance with the order of magnitude of observed growth rates.[11,12]

These experimental observations about the growth and rise of bubbles were first done by Shafer and Zare with bubbles rising and growing in a glass of beer.[30] They were also very recently confirmed by Zhang and Xu, who proposed a model for the growth rate of rising bubbles in both champagne and beer.[31]

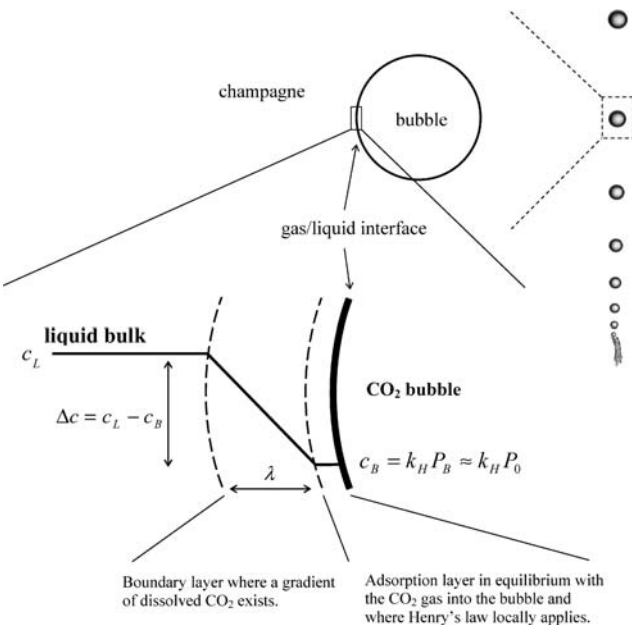

Fig. 20 Carbon dioxide concentrations in the close vicinity of the CO_2 bubble surface.

4.2. Average bubble size

Because champagne and sparkling wine tasters are often concerned with the size of bubbles formed in the wine (a proverb says that the smaller the bubbles, the better the wine), much attention was paid recently to model the average size of ascending bubbles. Actually, the final average size of ascending bubbles is the result of a combination between their growth rate and their ascending velocity. Recent calculations, based on mass transfer equations, linked the final average bubble size with various physicochemical and geometrical parameters.[3,22] The following dependence of the ascending bubble radius R on some of the liquid parameters was derived (in the MKSA system):

$$R \approx 1.24 \left(\frac{9\eta}{2\alpha\rho g}\right)^{2/9} \left(\frac{\Re\theta}{P_\mathrm{B}}\right)^{1/3} D_0^{2/9} (\Delta c)^{1/3} h^{1/3} \qquad (24)$$

Minute details about the exact determination of eqn (24) can be found in ref. 22. To go further with the dependence of bubbles' radii on some few parameters, we can also replace in eqn (24) the diffusion coefficient D_0 by its theoretical expression approached through the well-known Stokes–Einstein equation ($D_0 \approx k_\mathrm{B}\theta/6\pi\eta d$). The following relationship expressed in the MKSA system was thus obtained:

$$R(h, \theta, \ldots) \approx 2.5 \left(\frac{3k_\mathrm{B}}{4\pi\alpha r}\right)^{2/9} \left(\frac{1}{\rho g}\right)^{2/9} \left(\frac{1}{P_0}\right)^{1/3} \theta^{5/9} (c_\mathrm{L} - c_\mathrm{B})^{1/3} h^{1/3} \qquad (25)$$

It is worth noting that the dependence of the bubble size on the liquid viscosity vanishes. Finally, by replacing in eqn (25), k_B, α, and d by their known numerical values, and by developing c_B as $k_\mathrm{H} P_0$, one obtains:

$$R \approx 2.7 \times 10^{-3} \theta^{5/9} \left(\frac{1}{\rho g}\right)^{2/9} \left(\frac{c_\mathrm{L} - k_\mathrm{H} P_0}{P_0}\right)^{1/3} h^{1/3} \qquad (26)$$

Otherwise, because the liquid density ρ does not significantly vary from one champagne to another (and even from one carbonated beverage to another), we will discuss and put the accent on the influence of the following parameters on the bubble size: (i) the travelled distance h, (ii) the liquid temperature θ, (iii) the gravity acceleration g, (iv) the ambient pressure P_0, and (v) the carbon dioxide content c_L.

(i) The longer the travelled distance h, the larger the bubble size. This dependence of the bubble size on its travelled distance through the liquid means that, during champagne tasting, the average bubble size at the champagne surface varies from one glass to another. In a narrow flute, for example, the level of champagne poured is about three times higher than that in a typical coupe (with a shallower bowl and a much wider aperture). Therefore, the average bubble diameter in the flute will be larger than that in the coupe by a factor of about $R_{flute}/R_{coupe} \approx 3^{1/3} \approx 1.45$ (*i.e.*, bubbles about three times larger in volume!).

(ii) In eqn (26), the temperature appears directly as $\theta^{5/9}$, but we should not forget that the Henry's law constant k_H is also strongly temperature-dependent (see Fig. 2) and conveniently expressed by the Van't Hoff eqn (3). The temperature being expressed in K, the temperature dependence of the bubble size is nevertheless quite weak. Increasing the liquid temperature by 10 K (let's say from 278 to 288 K, which is approximately the range of champagne tasting temperature) makes bubbles grow only about 5–6% in diameter.

(iii) The gravity acceleration which is the driving force behind the bubble rise (through buoyancy) also plays a quite important role in the final bubble size. This could indeed be easily evidenced during a parabolic flight where the acceleration changes from micro-gravity (close to zero g) to macro-gravity (up to 1.8 g). On the Moon for example, where the gravity is about 1/6 the gravity on Earth, the average bubble size would increase by a factor of about $g_{Moon}/g_{Earth} \approx 6^{2/9} \approx 1.49$ (*i.e.*, bubbles almost 50% larger in diameter and therefore more than 3 times larger in volume).

(iv) The pressure inside the rising bubble is equivalent to the ambient pressure P_0 (for the reasons detailed in the section above). Usually, at sea level, this pressure is equivalent to 1 atm (or 10^5 N m^{-2}). Reducing the atmospheric pressure to only 0.3 atm (on the top of Mount Everest, for example) would increase the average bubble diameter by about 55% (and therefore by a factor of almost 4 in volume). This is basically the same phenomenon which is responsible for gas embolism in divers who have breathed high-pressure air under water if they resurface too quickly.

(v) The carbon dioxide content of the liquid medium c_L also influences the final average bubble size. This is the main reason why bubbles in beer are significantly smaller than bubbles in champagne and sparkling wines. Actually, the carbon dioxide content in beers may classically vary from about 4 g L^{-1} to 7 g L^{-1}, whereas the carbon dioxide content in champagne and sparkling wines may vary from 10 g L^{-1} up to 12 g L^{-1} (*i.e.*, c_L is approximately 2 times higher in champagne than in beer). Reducing c_L by a factor 2 in eqn (26) would decrease the theoretical average bubble size by about 40% (thus leading to bubbles almost 5 times smaller in volume). The two photographs displayed in Fig. 21 illustrate the significant difference in bubble size between a standard commercial champagne and a standard commercial beer, both showing very typical bubbling behaviour.

Moreover, after pouring champagne into a flute, due to bubbling and diffusion through the surface of champagne, CO_2 molecules progressively escape from the liquid medium. Subsequently, the dissolved carbon dioxide content c_L in the liquid medium progressively decreases. Therefore, as time proceeds during champagne tasting, the average bubble size at the liquid surface progressively decreases, as can be clearly seen in the sequence displayed in Fig. 22.

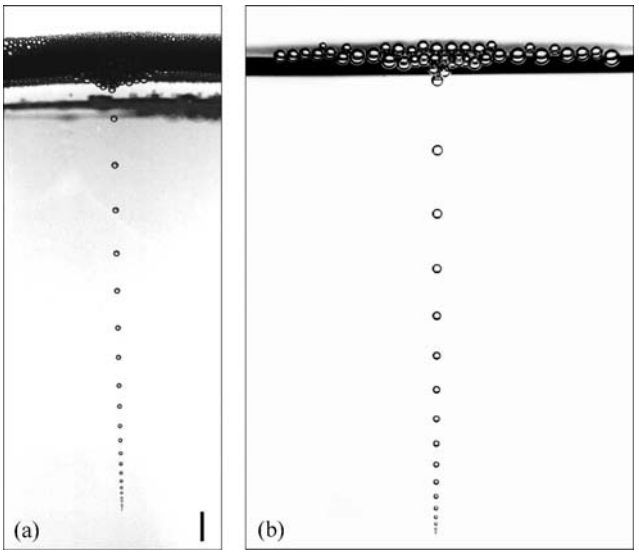

Fig. 21 Three minutes after pouring, bubbles rising in a glass of beer (a) show diameters much lower than those of bubbles rising in a flute poured with champagne (b) (bar = 1 mm); the very significant difference between the bubble size in champagne and beer is mainly due to amounts of dissolved-CO_2 about two times higher in champagne than in beer. (Photographs by Gérard Liger-Belair.)

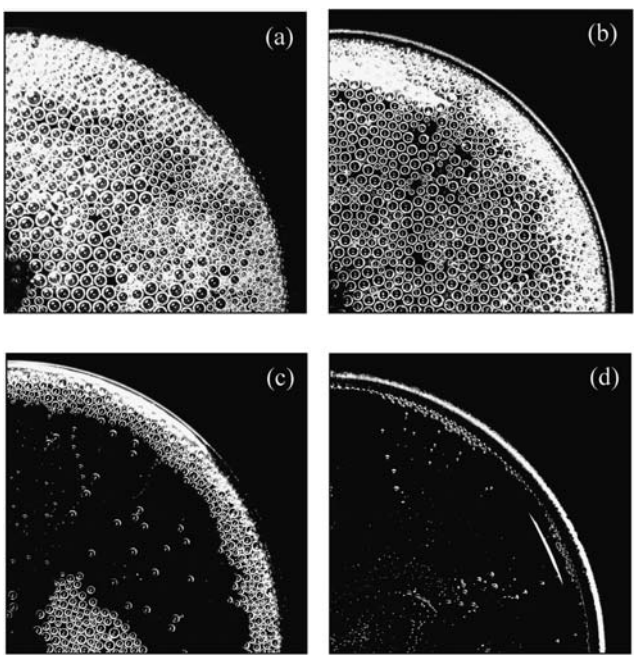

Fig. 22 Time sequence showing successive top views of a flute poured with champagne and followed as time proceeds; (a) immediately after pouring, (b) 3 min after pouring, (c) 10 min after pouring, and (d) 25 min after pouring; it clearly appears that the average bubble size decreases as time proceeds, as well as the average number of floating bubbles. (Photographs by Gérard Liger-Belair.)

4.3. Evidence for flow patterns, and their likely impact on champagne tasting

During champagne or sparkling wine tasting, consumers certainly pay attention to the continuous flow of ascending bubbles (often even before smelling and tasting the wine). Ascending bubbles are indeed visually appealing, but in the case of champagne tasting, their role is suspected to go far beyond the solely aesthetical point of view. Actually, at the bubble scale, the lower part of a rising bubble is a low pressure area which literally attracts the fluid molecules around (see Fig. 23). A rising bubble is thus able to drain some fluid along its path toward the free surface. The huge number of bubbles released from the numerous nucleation sites found in a typical champagne glass (in the order of several hundreds of bubbles released per second during the first minutes of champagne tasting) is therefore able to set the whole liquid bulk in motion.

Very recently, it was demonstrated that ascending bubbles act like many swirling motion generators in champagne glasses.[28,32] Together with Professor Guillaume Polidori and Fabien Beaumont from Reims University, laser tomography techniques were used in order to visualize, as accurately as possible, the flow patterns induced by the continuous flow of ascending bubbles in flutes poured with champagne. The principle of the experiment is to generate a 2 mm-thick laser sheet, built from a multi-line argon laser source (INNOVA 70C–2W) centred on the 514 nm wavelength. The 2 mm-thick laser sheet crosses the plane of symmetry of a champagne glass. Before pouring champagne into the glass, the champagne was seeded with tiny and roughly spherical particles (called Rilsan® particles). Rilsan particles are polymeric materials which exhibit a high degree of reflectivity with regard to the laser wavelength and are therefore able to diffuse the laser light as they cross the 2 mm-thick laser sheet. Rilsan particles are neutrally buoyant (75 μm < diameter < 150 μm; $\rho = 1.06\ \mathrm{g\ cm^{-3}}$). Moreover, Rilsan particles were found to be completely neutral with regard to bubble formation (this was definitely a crucial condition for the feasibility of the work). Classical long exposure time photography of the laser sheet was used in order to follow the motion of Rilsan particles, thus freezing the flow patterns inside the fluid section crossed by the laser sheet. Trajectories of convection currents in champagne glasses were therefore made visible by numerous streaks of light left by the Rilsan particles along their path through the laser sheet. A photograph of the optical workbench used to capture the champagne flow patterns is displayed in Fig. 24. In Fig. 24, the laser sheet boundaries are made visible by solid blue lines.

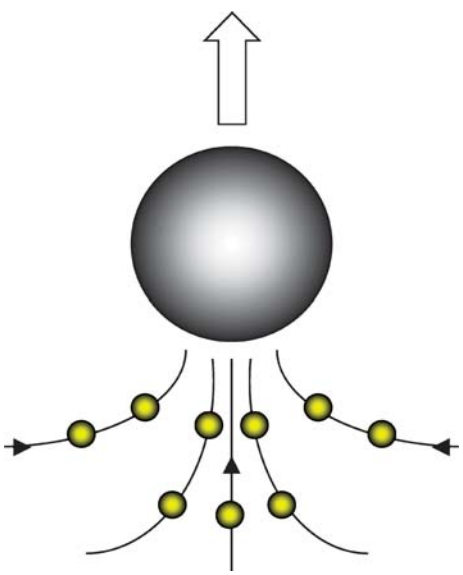

Fig. 23 A rising bubble is able to drain some fluid along its path through the champagne bulk.

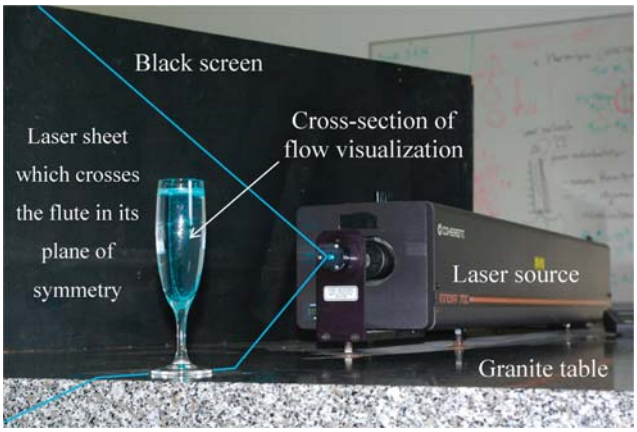

Fig. 24 Photograph of the optical workbench used to capture the champagne flow patterns; the laser sheet boundaries are made visible by solid blue lines.

The stability of flow patterns was investigated in flutes showing natural as well as artificial effervescence, throughout the first fifteen minutes after pouring. Both engravement

Fig. 25 Typical time sequence showing the flow patterns found in the plane of symmetry of a flute showing natural effervescence; a detail of the swirling motion (framed with white) is enlarged above the time sequence. (Photographs by G. Liger-Belair, F. Beaumont and G. Polidori.)

conditions and glass-shape were found to strongly influence the kinetics and the stability with time of the mixing flow phenomena found in champagne glasses. In Fig. 25, three successive frames of a typical time-sequence showing the flow patterns found in the flute showing natural effervescence are displayed. Throughout the first fifteen minutes which follow the pouring process, champagne is found to be mechanically mixed by various convection currents, made visible by the movement of the neutrally buoyant Rilsan particles which freeze the fluid motion during the 2 s exposure time of our digital photo camera. It is worth noting that the various convection cells and eddies found in the flute may change randomly in size and location with time. Convection currents induced by the flow of ascending bubbles are not at all stable with time. Actually, in a flute showing natural effervescence, bubbles arise from nucleation sites located randomly on the flute's wall. Furthermore, bubbles may also arise from nucleation sites directly found in the liquid bulk (called fliers and presented in section 3.6).[25] The natural ''bubbling environment'' is therefore highly random. This is the reason why the mixing flow mechanisms, directly induced by the random distribution of bubble nucleation sites, are highly complex and not at all stable with time in a flute showing natural effervescence.

In Fig. 26, three successive frames of a typical time-sequence showing the flow patterns found in a flute engraved at its bottom are displayed. It is clear that strong differences appear in the flow behaviour according to whether the glass has sustained or not a specific surface treatment. Actually, due to the high degree of reflectivity of bubbles with regard to the laser wavelength, one clearly observes the formation of the rising gas column along the vertical axis of symmetry of the flute (from the treated bottom surface up to the free surface of champagne). One can also clearly notice from Fig. 26 that the rising bubble column generates two large and well-established vortices which are very stable, and last throughout the first fifteen minutes after pouring. Actually, because the flute exhibits cylindrical symmetry around its central axis, the real three dimensional structure of the flow patterns in the bulk of the engraved flute is that of a deformed torus. Therefore, and contrary to the case of the flute showing natural effervescence, the convection currents found within the engraved flute are very stable with time. The main reason is that the ascending liquid flow generated by the rising central bubbles column largely exceeds the other contributions to the liquid flow generated by the likely presence of single bubble trains randomly distributed within the glass. The main convection currents are undoubtedly forced by this intense and artificial effervescence. Moreover, it is worth noting that, in the case of the engraved champagne flute, the whole domain of the champagne bulk is homogeneously mixed, with high values for the average fluid velocities, throughout the fifteen minutes which follow the pouring process.

To complement the previous flow visualization method, to better highlight the vortical structures and to access the streak-line patterns of the champagne flow found inside an engraved flute, another method based on dye dispersion was used (see the laser tomography displayed in Fig. 27). Fluorescent dyes of sulforhodamine and fluorescein have carefully been injected in the champagne section crossed by

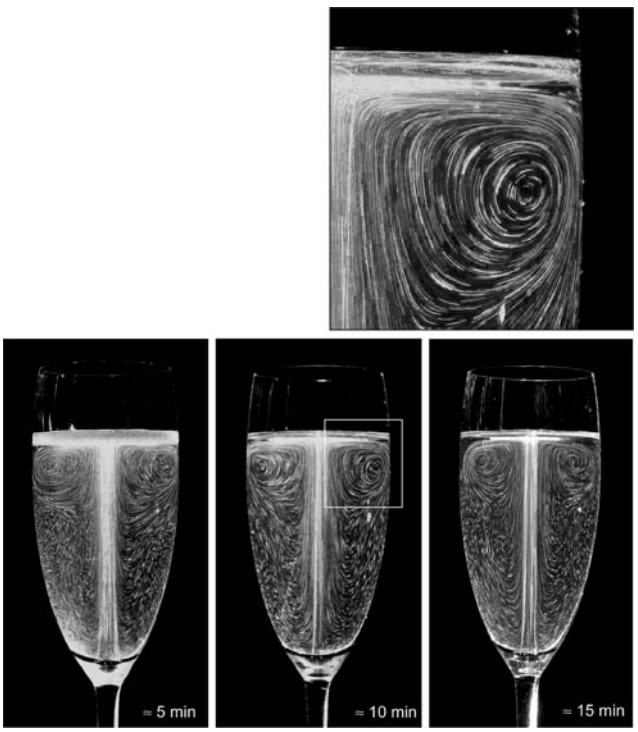

Fig. 26 Typical time sequence showing the flow patterns found in the plane of symmetry of a flute engraved at its bottom (with a ring-shaped engravement similar to that displayed in Fig. 18); a detail of the swirling motion (framed with white) is enlarged above the time sequence. (Photographs by G. Liger-Belair, F. Beaumont and G. Polidori.)

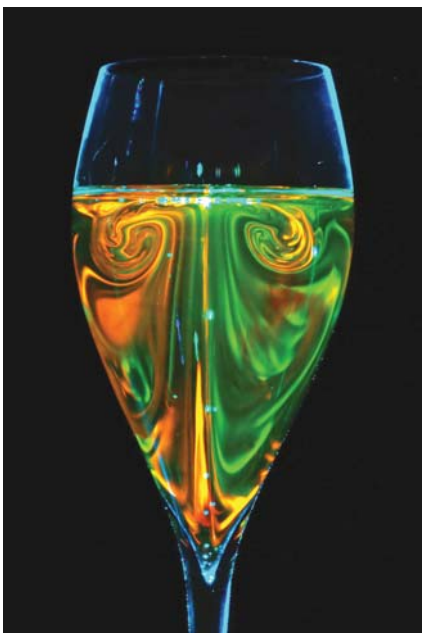

Fig. 27 Flow patterns found inside an engraved champagne flute as highlighted by use of fluorescent dyes injected in the flute section crossed by the laser sheet: sulforhodamine (left), and fluorescein (right). (Photograph by G. Liger-Belair, F. Beaumont and G. Polidori).

the laser sheet after champagne was poured to highlight the flow patterns without requiring the use of Rilsan particles.

Significant differences concerning the mixing flow patterns within the champagne bulk were also found between an engraved flute and an engraved coupe. In the case of an engraved champagne coupe, only about half of the liquid medium was found to be mixed by the flow of ascending bubbles arising from the bottom of the coupe (see Fig. 28). The external periphery of the coupe is characterized by a "dead-zone" where champagne is almost at rest.[28,32] Therefore, it is clear that both glass-shape and engravement conditions influence the overall characteristics of mixing flow phenomena found in champagne glasses.

By vigorously and continuously mixing the liquid medium throughout tasting, ascending bubbles are indeed suspected to play a major role in flavour and gas release. Actually, the flavour and gas release from the wine interface is a diffusion process which is therefore ruled by the so-called Fick's law, expressed as follows:

$$\overrightarrow{J}_i = c_i \overrightarrow{V} - D_i \overrightarrow{\nabla} c_i \qquad (27)$$

where $\vec{J}_i$, $\vec{V}$, c_i, $\overrightarrow{\nabla} c_i$, and D_i are the flux of a given compound i through the gas/liquid interface, the velocity field of the liquid flow near the wine interface, the bulk concentration of the given compound, the concentration gradients of the given compound close to the interface, and the diffusion coefficient of the given compound in the champagne bulk, respectively. It is clear from eqn (27) that both gas discharge and flavour release are highly fluid velocity-dependent through the parameter $\vec{V}$. Therefore, to better approach the kinetics of flavour and gas release from glasses poured with champagne and sparkling wines, the velocity field close to the wine interface needs to be better known throughout the tasting process.

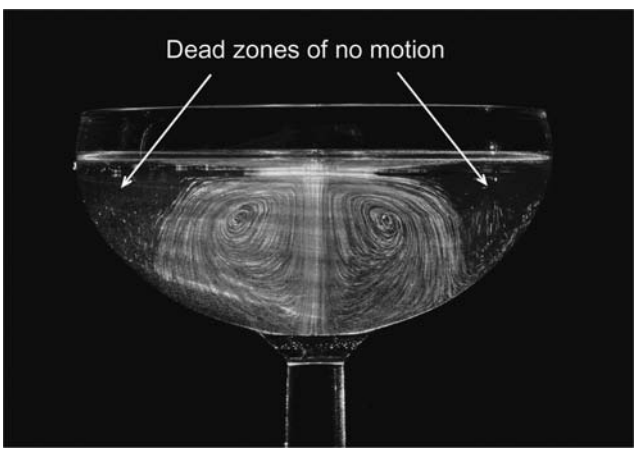

Fig. 28 Flow patterns found in the plane of symmetry of a coupe engraved at its bottom (with a ring-shaped engravement similar to that displayed in Fig. 18); it can be seen that, as for the flute engraved at its bottom, the rising bubble column forces the flow patterns into the form of two counter-rotative vortices close to the glass axis; nevertheless, in this case, the external periphery of the glass is characterized by a dead-zone where the champagne is almost at rest; it means that, for such a wide-brimmed glass, only about half of the liquid bulk participates to the champagne mixing process. (Photograph by G. Liger-Belair, F. Beaumont and G. Polidori.)

In the near future, we plan to accurately investigate the velocity field in various other models of champagne glasses showing natural as well as artificial effervescence. We plan to test various glass shapes (the inventive spirit of glassmakers is fertile in this field) as well as various engravement conditions. Actually, the modern techniques of glass engravement, done to promote effervescence, enable various models of engravement (in terms of shape and location in the glass), thus logically modifying the overall convection currents conditions induced by artificial effervescence. Moreover, since we strongly suggest close links between the kinetics of convection currents and the kinetics of flavour and CO_2 release, quantitative measurements of the kinetics of CO_2 and volatile organic compounds discharged from various champagne glasses under various glass-shape and engravement conditions are also to be conducted, together with sensory analysis experiments.

5. Close-up on bubbles bursting at the liquid surface

5.1. The bursting process as frozen by high-speed photography

A champagne bubble reaches the liquid surface with a size that depends on the distance h travelled from its nucleation site, as expressed in eqn (26). Experimentally, it was observed that bubble diameters rarely exceed about 1 mm. At the free surface, the shape of a bubble results from a balance between two opposing effects: the buoyancy F_B, of the order of $\rho g \pi R^3$, which tends to make it emerge from the liquid surface and a capillary force F_C inside the hemispherical thin liquid film, of the order of $\sigma \pi R$, which tends to maintain the bubble below the liquid surface. In the case of champagne millimetric bubbles, buoyancy will be neglected in front of capillary effects. Consequently, like a tiny iceberg, a bubble only slightly emerges from the liquid surface, with most of its volume remaining below the free surface. The emerged part of the bubble, the bubble-cap, is essentially a spherically shaped film of liquid, which gets thinner and thinner as the liquid drains back into the liquid bulk. A bubble-cap which has reached a critical thickness of about 100 nm becomes so thin and sensitive to such disturbances as vibrations and temperature changes that it finally ruptures.[33] For bubbles of millimetre size, the disintegration of the bubble-cap takes from 10 to 100 μs. During this extremely brief initial phase, the bulk shape of the bubble is literally "frozen", and a nearly millimetric open cavity remains as a tiny indentation in the liquid surface (see the high speed photograph displayed in Fig. 29). Then, a complex hydrodynamic process ensues, causing the collapse of the submerged part of the bubble and projecting into the air a liquid jet which quickly breaks up into tiny droplets of liquid (called jet drops). This process is indeed characteristic of every carbonated beverage. Generally speaking, the number, size, and velocity of jet drops produced during bubble collapse depend on the size of the initial bursting bubble.[34–37] In Fig. 30, the close-up high speed photograph of a tiny liquid jet caused by the collapse of a champagne bubble is displayed.[38]

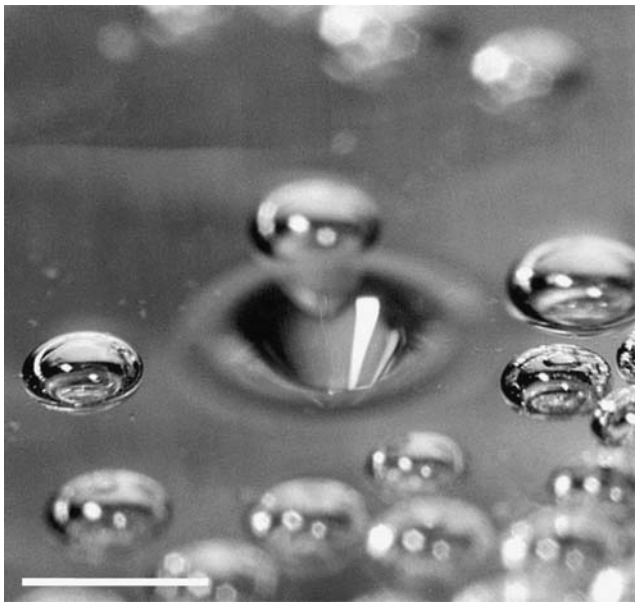

Fig. 29 The bubble-cap of a bubble at the champagne surface has just ruptured (on a time-scale of 10 to 100 μs); during this extremely brief initial phase, the bulk shape of the bubble has been "frozen", and a nearly millimetric open cavity remains as a tiny indentation in the liquid surface (bar = 1 mm). (Photograph by Gérard Liger-Belair.)

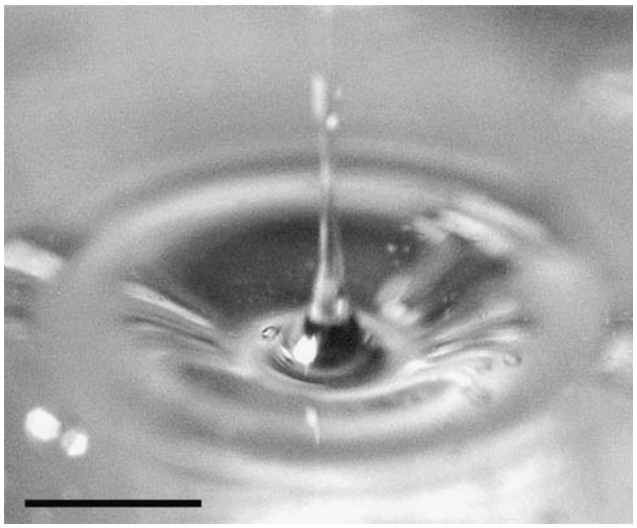

Fig. 30 The collapsing bubble cavity gives rise to a high-speed liquid jet above the champagne surface (bar = 1 mm). (Photograph by Gérard Liger-Belair.)

It was also found that the "olfactive" role of bubbles does not only concern the mixing mechanism of the liquid phase presented in the above section. Actually, the myriad of bubbles bursting at the liquid surface radiate hundreds of tiny liquid jets which quickly break up into a multitude of tiny droplets every second, thus forming a cloud of droplets above the champagne surface, as shown in the photograph displayed in Fig. 31. Those tiny droplets, ejected up to several centimetres above the liquid surface, partly evaporate themselves, thus accelerating the transfer of the numerous aromatic volatile organic compounds above the liquid surface. This very

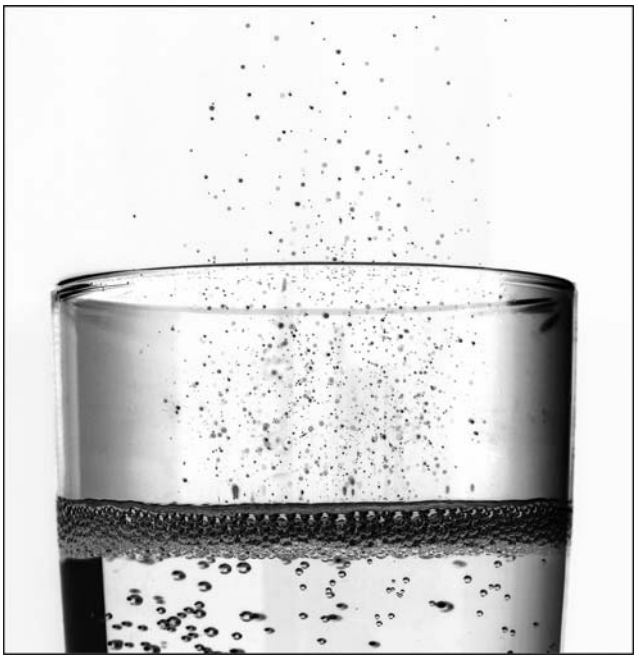

Fig. 31 The collapse of hundreds of bubbles at the free surface radiates a cloud of tiny droplets which is characteristic of champagne and sparkling wines and which complements the sensual experience of the taster (© Alain Cornu/Collection CIVC).

characteristic fizz considerably enhances the flavour release in comparison with that from a flat wine for example. Laser tomography techniques were applied to freeze the huge number of bursting events and the myriad of droplets ejected above champagne glasses in real consuming conditions (see the tomography of the droplets' cloud above the surface of a coupe displayed in Fig. 32).[39]

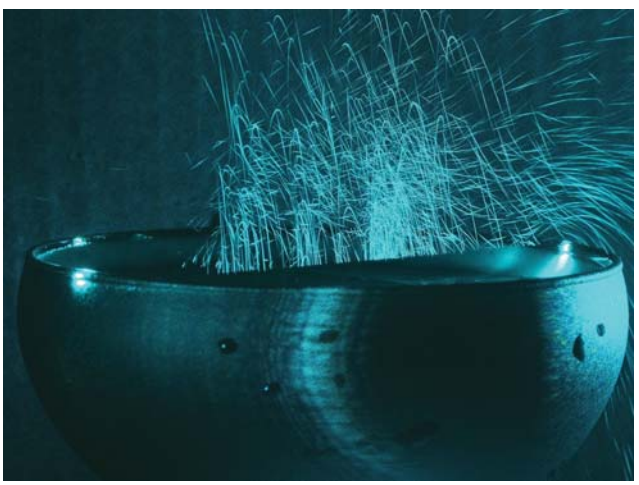

Fig. 32 The cloud constituted by myriads of tiny droplets ejected from bubbles bursting above the surface of a coupe, as seen through laser tomography technique; the droplets' trajectories are materialised by blue streaks of light during the 1 s exposure time of a digital photo camera. (Photograph by G. Liger-Belair, F. Beaumont and G. Polidori.)

5.2. When champagne bubbles dress up like flowers...

The close observation of bubbles collapsing at the free surface of a glass poured with champagne also revealed another unexpected and lovely phenomenon. A few seconds after pouring, and after the collapse of the foamy head, the surface of a champagne flute is covered with a layer of bubbles—a kind of bubble raft, also called bi-dimensional foam, where each bubble is generally surrounded by six neighbouring bubbles (see Fig. 33).[40] Scientifically speaking, bubbles arrange themselves in an approximately hexagonal pattern, strikingly resembling those in beeswax. While snapping pictures of the bubble raft after pouring, I also accidentally took some pictures of bubbles collapsing close to one another in the raft. When the bubble-cap of a bubble ruptures and leaves an open cavity at the free surface, adjacent bubble-caps are sucked towards this empty cavity and create unexpected and short-lived flower-shaped structures, unfortunately invisible to the naked-eye (see the high speed photograph displayed in Fig. 34).[41,42] Shear stresses induced by bubbles trapped in the close vicinity of a collapsing one are even better visualized on the high-speed photograph displayed in Fig. 35, where the bubble raft is not complete. Such behaviour first appeared counter-intuitive to me. Paradoxically, adjacent bubble-caps are sucked and not blown-up by bursting bubbles, contrary to what could have been expected at first glance.

Actually, after the disintegration of a bubble-cap, the hexagonal symmetry around adjoining bubbles is suddenly locally broken. Therefore, the symmetry in the field of capillary pressure around adjoining bubbles is also locally broken. Capillary pressure gradients all around the now empty cavity are detailed in Fig. 36. Signs +/− indicate a pressure

Fig. 33 A few seconds after pouring, and after the collapse of the foamy head, the surface of a champagne flute is covered with a layer of quite monodisperse millimetric bubbles, where bubbles arrange themselves in an approximately hexagonal pattern, strikingly resembling those in beeswax (bar = 1 mm). (Photograph by Gérard Liger-Belair.)

Fig. 34 Flower-shaped structure found during the collapse of bubbles in the bubble raft at the free surface of a flute poured with champagne (bar = 1 mm). (Photograph by Gérard Liger-Belair.)

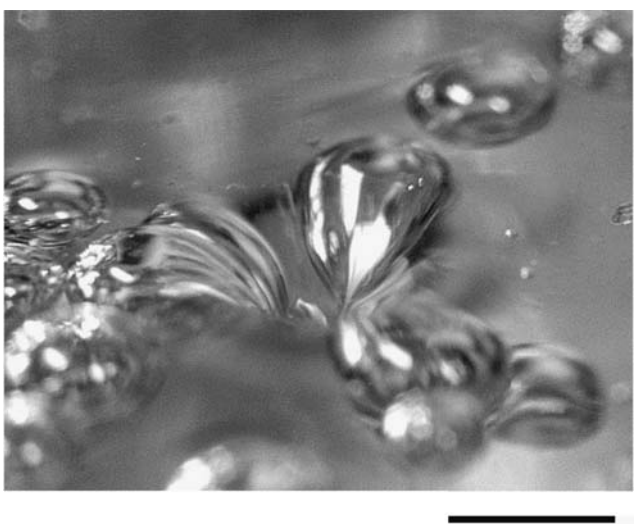

Fig. 35 Shear stresses experienced by bubbles adjacent to a collapsing one at the free surface of a flute poured with champagne (bar = 1 mm). (Photograph by Gérard Liger-Belair.)

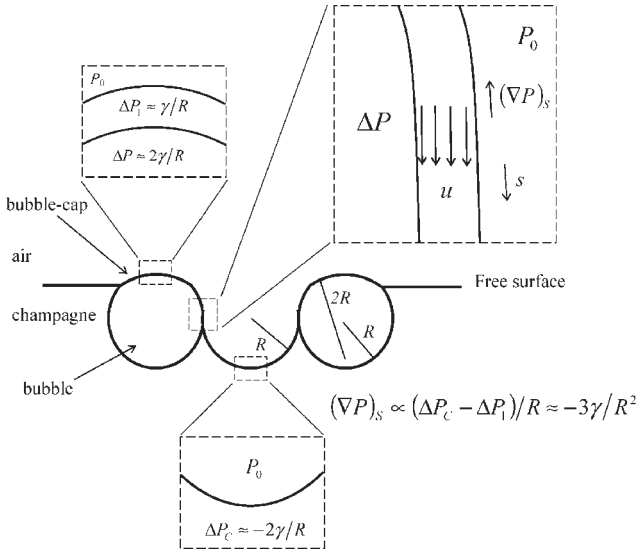

Fig. 36 Schematic transversal representation of the situation, as frozen after the disintegration of the central bubble-cap.

above/below the atmospheric pressure P_0. Finally, inertia and gravity being neglected, the full Navier–Stokes equation applied to the fluid within the thin liquid film of adjoining bubble-caps drawn by capillary pressure gradients, reduces itself to a simple balance between the capillary pressure gradients and the viscous dissipation as follows,

$$\eta(\Delta \vec{u})_S = (\vec{\nabla} P)_S \qquad (28)$$

where u is the velocity in the thin liquid film of adjacent bubble-caps, η is the champagne viscosity, $\vec{\nabla} P$ are the capillary pressure gradients, and s is the axial coordinate which follows the bubble-cap's curvature and along which the fluid within the thin film is displaced.

The asymmetry in the capillary pressure gradients distribution around a bubble-cap adjacent to an empty cavity is supposed to be the main driving force of the violent sucking process experienced by a bubble-cap in touch with a bursting bubble. Actually, due to higher capillary pressure gradients, the liquid flows that develop in the half of the bubble-cap closest to the open cavity are thus expected to be higher than those which develop in the rest of the bubble-cap. It ensues a violent stretching of adjoining bubble-caps toward the now empty cavity, which is clearly visible in the photographs displayed in Fig. 34 and 35.

More recently, those flower-shaped structures have been observed during the coarsening of bi-dimensional aqueous foams, obtained by mixing a surfactant, sodium dodecyl sulfate (SDS), with pure water.[43] But it is worth noting that this lovely and short-lived process was first done at the top of a champagne flute.[41] Many fascinating processes in nature are often hidden behind everyday phenomena such as those found in a simple flute poured with champagne.[44]

5.3. Avalanches of bursting events in the bubble raft?

Actually, avalanches of popping bubbles were put in evidence during the coarsening of bi-dimensional and three dimensional aqueous foams.[43,45,46] How does the bubble raft behave at the surface of a flute poured with champagne? Does a bursting bubble produce a perturbation which extends to the neighbouring bubbles and induce avalanches of bursting events which finally destroy the whole bubble raft? In the case of champagne wines, a few time sequences of bubbles bursting in the bubble raft have been captured with a high-speed video camera. One of them is displayed in Fig. 37. Between frame 1 and frame 2, the bubble pointed with the black arrow has disappeared. In frame 2, neighbouring bubbles are literally sucked toward this now bubble-free area. Then, neighbouring bubbles oscillate for a few milliseconds and progressively recover their initial hemispherical shape. In conclusion, in the case of bubbles adjacent to collapsing ones, despite high shear stresses produced by a violent sucking process, bubbles adjacent to collapsing ones were never found to rupture and collapse in turn, thus causing a chain reaction. At the free surface of a flute poured with champagne, bursting events appear to be spatially and temporally non-correlated. The absence of avalanches of bursting events seems to be linked to the champagne viscosity (which is about 50% higher than that of pure water).[43] It can also be noted that a tiny daughter bubble, approximately ten times smaller than the initial central bubble, has been entrapped during the collapsing process of the central cavity (as clearly seen in frames 4 and 5 of Fig. 37).

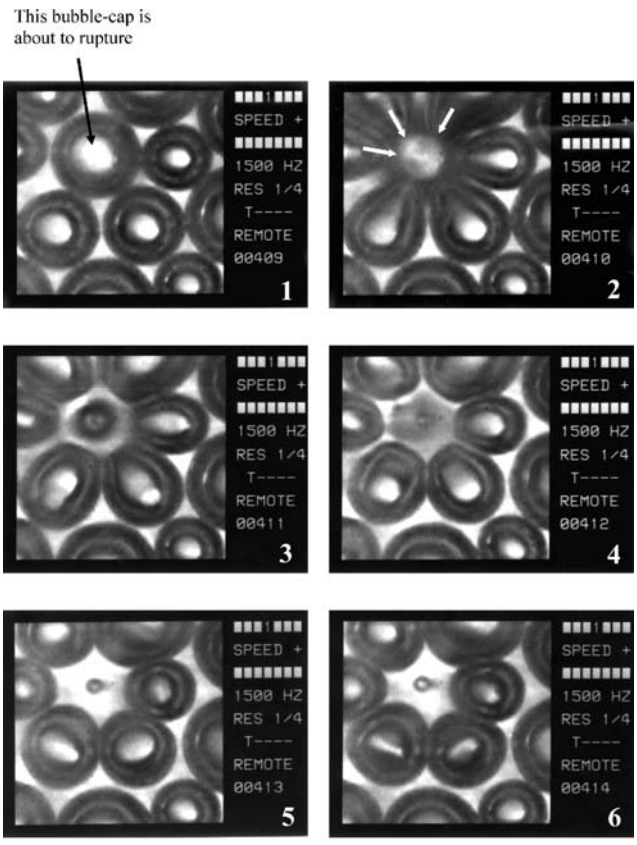

Fig. 37 Time sequence illustrating the dynamics of adjoining bubbles in touch with a collapsing one at the free surface of a flute poured with champagne; the whole process was filmed at 1500 frames s^{-1}; from frame 4, in the centre of the empty cavity left by the collapsing bubble, a tiny air-bubble entrapment is observed (bar = 1 mm). (Photographs by Gérard Liger-Belair.)

Fig. 38 The liquid-jet deviates from vertical as the neighbouring bubbles' symmetry is broken around a collapsing bubble (bar = 1 mm). (Photograph by Gérard Liger-Belair.)

Bubble entrapment during the collapsing process was already experimentally and numerically observed with single millimetric collapsing bubbles,[47,48] including champagne bubbles.[38]

5.4. A particular situation: as the jet deviates from vertical

The photograph displayed in Fig. 38 finally illustrates the alluring of the liquid jet in a quite particular situation. On the right side of this picture, the collapsing bubble is bordered by three neighbouring bubbles, whereas on the left side, there are no adjoining bubbles. The hexagonal symmetry is broken. In this case, the tiny liquid jet (previously perfectly vertically oriented, as in Fig. 30) deviates from vertical.[49] The jet is deviated toward the ''bubble-free'' area. There are certainly no enological consequences of such a situation, but experts in the science of bubbles and foams ask themselves why such a deviation from vertical is observed...

To end this critical review about the latest advances in the science of champagne bubbles, Gérard Liger-Belair would like to pay homage to two scientists who inspired him so much when he was a student: the recently deceased Professor Pierre-Gilles de Gennes (1932–2007), Nobel Prize in Physics in 1991, and Doctor Harold Edgerton, the twentieth century master of stop-action photography. Prof. de Gennes was a pioneering scientist who invented and developed a new area of science devoted to what we call today ''soft matter''. His contribution to the science of thin films, bubbles and foams is huge. He recently wrote, together with two renowned colleagues, a wonderful book, which provides numerous answers to common questions about everyday phenomena.[50] Dr Harold Edgerton (1903–1990) revealed to the general public the beauty of ''high-speed events'' and inspired generations of young scientists. Dr Edgerton devoted his entire career to recording what the unaided eye cannot see, in order to reveal the laws of nature.[51] His most famous snapshot, the coronet made by a drop of milk, is familiar to millions of people throughout the world, and has become an icon and hallmark of the juncture between pure science and modern art. ''*The experience of seeing the unseen has provided me with insights and questions my entire life*'', told Harold Edgerton. This sentiment exactly captures the heart of the matter. Who could have thought at first glance that a flute poured with champagne could turn into such a fantastic playground for a physicist in love with high-speed microphotography, and for any champagne lover with the knowledge and time to reflect.

Acknowledgements

This research was partially supported by the Europol'Agro institute and by the Conseil Général de la Marne. The authors warmly thank Fabien Beaumont, from Reims University, for valuable discussions and for his precious help concerning the recent and exciting experiments conducted with laser tomography techniques. The authors are grateful to the team of the Laboratoire d'Oenologie et Chimie Appliquée, for their constant help and valuable discussions. Thanks are also due to Champagne Moët & Chandon and Champagne Pommery for regularly supplying us with wine samples, to ARC-International for supplying us with various and up-to-date glasses, and to Jean-Claude Colson and AROCU for encouragements and for supporting our research. The authors are finally also grateful to the CIVC for providing the photograph displayed in Fig. 1, and to Jacques Honvault for providing the high-speed photograph displayed in Fig. 5.

References

1 G. Liger-Belair, *Uncorked: The Science of Champagne*, Princeton University Press, Princeton New Jersey, 2004.
2 G. G. Agabaliantz, *Bull. O.I.V.*, 1963, **36**, 703.
3 G. Liger-Belair, *J. Agric. Food Chem.*, 2005, **53**, 2788.
4 D. R. Lide and H. P. Frederikse, *CRC Handbook of Chemistry and Physics*, CRC Press, Boston, 76th edn, 1995.
5 A. Dussaud, *Etude des propriétés de surface statiques et dynamiques de solutions alcooliques de protéines: Application à la stabilité des mousses de boissons alcoolisées*, PhD Thesis, ENSIAA, Massy France, 1993.
6 G. Autret, G. Liger-Belair, J.-M. Nuzillard, M. Parmentier, A. Dubois de Montreynaud, P. Jeandet, B. T. Doan and J.-C. Beloeil, *Anal. Chim. Acta*, 2005, **535**, 73.
7 S. D. Lubetkin and M. Blackwell, *J. Colloid Interface Sci.*, 1988, **126**, 610.
8 F. Lugli and F. Zerbetto, *Phys. Chem. Chem. Phys.*, 2007, **9**, 2447.
9 S. F. Jones, G. M. Evans and K. P. Galvin, *Adv. Colloid Interface Sci.*, 1999, **80**, 27.
10 S. D. Lubetkin, *Langmuir*, 2003, **19**, 2575.
11 G. Liger-Belair, *Ann. Phys. (Paris)*, 2002, **27**, 1.
12 G. Liger-Belair, M. Vignes-Adler, C. Voisin, B. Robillard and P. Jeandet, *Langmuir*, 2002, **18**, 1294.
13 G. Liger-Belair, R. Marchal and P. Jeandet, *Am. J. Enol. Vitic.*, 2002, **53**, 151.
14 G. Liger-Belair, C. Voisin and P. Jeandet, *J. Phys. Chem. B*, 2005, **109**, 14573.
15 S. Uzel, M. Chappell and S. Payne, *J. Phys. Chem. B*, 2006, **110**, 7579.

16 G. Liger-Belair, M. Parmentier and P. Jeandet, *J. Phys. Chem. B*, 2006, **110**, 21145.
17 M. Chappell and S. Payne, *J. Acoust. Soc. Am.*, 2007, **121**, 853.
18 A. O'Sullivan, *Cellulose*, 1997, **4**, 173.
19 R. Lucas, *Kolloid Z.*, 1918, **23**, 15.
20 E. Washburn, *Phys. Rev.*, 1921, **17**, 273.
21 G. Liger-Belair, D. Topgaard, C. Voisin and P. Jeandet, *Langmuir*, 2004, **20**, 4132.
22 G. Liger-Belair, *Ann. Phys. (Paris)*, 2006, **31**, 1.
23 G. Liger-Belair, A. Tufaile, B. Robillard, P. Jeandet and J.-C. Sartorelli, *Phys. Rev. E: Stat. Phys., Plasmas, Fluids, Relat. Interdiscip. Top.*, 2005, **72**, 037204.
24 G. Liger-Belair, A. Tufaile, P. Jeandet and J.-C. Sartorelli, *J. Agric. Food Chem.*, 2006, **54**, 6989.
25 G. Liger-Belair, F. Beaumont, P. Jeandet and G. Polidori, *Langmuir*, 2007, **23**, 10976.
26 A. D. Ronteltap, M. Hollemans, C. G. Bisperink and A. Prins, *Master Brew. Assoc. Am., Tech. Q.*, 1991, **28**, 25.
27 D. M. Lynch and C. W. Bamforth, *J. Food Sci.*, 2002, **67**, 2696.
28 G. Liger-Belair, J.-B. Religieux, S. Fohanno, M.-A. Vialatte, P. Jeandet and G. Polidori, *J. Agric. Food Chem.*, 2007, **55**, 882.
29 G. Liger-Belair, E. Prost, M. Parmentier, P. Jeandet and J.-M. Nuzillard, *J. Agric. Food Chem.*, 2003, **51**, 7560.
30 N. Shafer and R. Zare, *Phys. Today*, 1991, **44**, 48.
31 Y. Zhang and Z. Xu, *Elements*, 2008, **4**, 47.
32 G. Liger-Belair, F. Beaumont, M.-A. Vialatte, S. Jégou, P. Jeandet and G. Polidori, *Anal. Chim. Acta*, 2008, **621**, 30.
33 J. Senée, B. Robillard and M. Vignes-Adler, *Food Hydrocolloids*, 1999, **13**, 15.
34 D. E. Spiel, *J. Geophys. Res.*, 1995, **100**, 4995.
35 D. E. Spiel, *J. Geophys. Res.*, 1997, **102**, 5815.
36 D. E. Spiel, *J. Geophys. Res.*, 1998, **103**, 24907.
37 D. E. Spiel, *J. Geophys. Res.*, 1994, **99**, 10289.
38 G. Liger-Belair, H. Lemaresquier, B. Robillard, B. Duteurtre and P. Jeandet, *Am. J. Enol. Vitic.*, 2001, **52**, 88.
39 G. Liger-Belair and G. Polidori, *Pour La Science*, 2007, **362**, 66.
40 E. Zarifian, C. Coutant and G. Liger-Belair, *Bulle de champagne*, Perrin, Paris, 2005.
41 G. Liger-Belair, B. Robillard, M. Vignes-Adler and P. Jeandet, *C. R. Phys.*, 2001, **2**, 775.
42 G. Liger-Belair and P. Jeandet, *Langmuir*, 2003, **19**, 5771.
43 H. Ritacco, F. Kiefer and D. Langevin, *Phys. Rev. Lett.*, 2007, **98**, 244501.
44 E. Guyon, L. Petit and J.-P. Hulin, *Ce que disent les fluides*, Belin, Paris, 2005.
45 W. Müller and J.-M. di Meglio, *J. Phys.: Condens. Matter*, 1999, **11**, 209.
46 N. Vandewalle, J.-F. Lentz, S. Dorbolo and F. Brisbois, *Phys. Rev. Lett.*, 2001, **86**, 179.
47 J. Herman and R. Mesler, *J. Colloid Interface Sci.*, 1987, **117**, 565.
48 L. Duchemin, S. Popinet, C. Josserand and S. Zaleski, *Phys. Fluids*, 2002, **14**, 3000.
49 G. Liger-Belair, *Effervescence! La science du champagne*, Odile Jacob, Paris, 2006.
50 P.-G. De Gennes, F. Brochard-Wyart and D. Quéré, *Capillarity and Wetting Phenomena: Drops, Bubbles, Pearls, Waves*, Springer, New York, 2003.
51 E. Jussim, *Stopping Time: The Photographs of Harold Edgerton*, H. N. Abrams Inc., New York, 1987.